Analysis of surface variables and parameterization of surface processes in HIRLAM. Part I: Approach and verification by parallel runs

E. Rodríguez[1], B. Navascués[1], J.J. Ayuso[1] and S. Järvenoja[2]
[1] Spanish Meteorological Institute (INM), P.O. Box 275, 28070 Madrid, Spain
[2] Finnish Meteorological Institute (FMI), P.O. Box 503, 00101 Helsinki, Finland

(Manuscript received 23 September 2002, in final form 17 January 2003.)

Abstract

The analysis of surface variables and parameterization of surface processes of the reference HIRLAM system is described. Special emphasis has been put on the treatment of surface heterogeneity making that surface fluxes of heat and momentum inherit such high spacial variability. The so called "tiling" approach has been adopted to prevent the problems associated with the use of effective parameters in case of strongly changing surface conditions. The tiles are defined by coupling independently each homogeneous patch or "tile" of a grid square to the lowest level of the model. Tiles interact each other only through the atmosphere. Average surface fluxes are then computed by averaging surface fluxes over each land-use tile weighted by their fractional area. The model allows up to five different tiles (water, sea ice, bare ground, low vegetation, forest) within each grid square. Fractional snow cover is also allowed within each tile. The ISBA scheme has been selected to model land surface processes.

The surface analysis initializes the following surface variables: sea surface temperature (SST), fraction of water and ice, snow depth, 2-metre temperature, 2-metre relative humidity, surface soil temperature, mean soil temperature, surface soil water content and total soil water content. The algorithm is able to cope with the tiled structure by averaging some variables only over land tiles. SST and snow depth analyses are based on the successive correction method. 2-metre temperature and relative humidity analyses are based on the optimal interpolation method. Finally, soil water content analysis is based on the sequential method, which corrects water content depending on 2-metre temperature and relative humidity forecast errors, only in those synoptic cases where screen variables are strongly influenced by the surface beneath.

A comprehensive list of parallel runs covering all seasons of the year have been conducted to demonstrate the superiority of the new package against the previous surface treatment. Special emphasis has been put on summer time and midlatitude regions were the influence of soil water content on screen temperature and humidity is extremely high.

Contents

1 Introduction

The importance of the exchange processes at all time scales between the earth surface and the atmosphere has been increasingly recognized during the recent years. The requirement of accurate forecasting of weather parameters, such as screen level temperature and humidity, wind in the boundary layer and precipitation, needs a realistic description both of the surface physiographic features and of the exchange processes of momentum and heat. A new treatment of the surface processes should take into account the following aspects of the atmosphere/surface interaction: i) the importance of soil water content controlling the partition of the net radiative energy reaching the soil between latent and sensible heat flux; ii) the role of vegetation allowing exchange of water between the atmosphere and soil at the root depth and iii) the high dependence of screen level temperature and humidity on initial specification of soil water content.

Over the last years some deficiencies of the HIRLAM system related with an insuficient treatment of surface processes (see Källen (1996) for a description of the old surface scheme) were repeatedly reported. The lack of vegetation over the land surface, the absence of any assimilation of soil water content, the lack of treatment of soil water freezing and thawing, the insuficient physiographic description, etc. were all degrading the forecasting of weather parameters. The new package includes treatment of heterogeneity and assimilation of surface variables, especially of soil moisture. A state-of-art land-surface scheme will improve significantly the modelling of near surface and boundary layer variables.

This technical report describes in detail both the parameterization of surface processes and the analysis of surface variables recently implemented in the HIRLAM reference system (version 5.2.0). Some aspects not described here, *e.g.*, the physiograpic databases used, the vegetation and soil related parameters for the ISBA model and the postprocessed surface parameters, can be found in the first formulation of the scheme (Bringfelt, 1996) and which are still valid with only minor changes. Section 2 provides a brief review of land surface parameterization schemes and the problems linked to the treatment of surface heterogeneity. Section 3 gives a general introduction to the analysis of surface variables. The criteria considered to select an appropriate land-surface scheme are discussed in Section 4. Section 5 gives a brief description of the treatment of heterogeneity based on the mosaic of tiles approach and of the ISBA code finally chosen to model surface processes over land fractions. Section 6 describes the surface analysis algorithm used for the different analized variables: water surface temperature, snow depth, 2-metre temperature, 2-metre relative humidity, soil temperatures and soil water content. In Section 7 some considerations in connexion with postprocessing and verification are discussed. Finally, Section 8 describes the experiments conducted to validate and verify the whole new code for surface analysis and surface parametrization. Parallel runs using different domains, horizontal resolutions and covering all seasons of year have been carried out to compare the new code against the previous surface treatment in HIRLAM.

2 Parameterization of surface processes in numerical weather prediction models

2.1 Heterogeneity in the surface cover

The surface heat and momentum fluxes, which provide the coupling between the atmosphere and the earth's surface, depend not only on atmospheric conditions but also on surface characteristics. The earth's surface shows a high spatial variability at all scales, as can be readily appreciated by examining soil, vegetation and land-use maps. Consequently, the surface fluxes inherit such high spatial variability. The resolution of current atmospheric numerical models varies from a few km (in mesoscale models) up to about 100 km (in general circulation models). Therefore, it is necessary to integrate the effects of spatial variability to obtain representative surface fluxes at the grid resolution of the atmospheric models.

The effects of surface inhomogeneities on the atmosphere depend on the horizontal scale of landscape variation. Shuttleworth (1988) suggested that for length scales smaller than about 10 km, no apparent impact of the surface inhomogeneities can be observed in the atmosphere since turbulence is very efficient at mixing the boundary layer. Li and Avissar (1994) illustrated the impact of microscale variability of land characteristics (including soil water content) on the surface heat fluxes by comparing averaged surface fluxes computed from different distributions of land surface parameters with surface fluxes computed from the corresponding distribution means. They found that latent heat flux was the most sensitive to spatial variability, and that radiative flux emitted by the surface was the least sensitive. They emphasized the importance of considering the spatial variability of leaf area index, stomatal conductance, and, in bare land, soil-surface water content to calculate accurately the surface fluxes. They also found that the more positively skewed the distribution within the range of land-surface characteristics that is non-linearly related to the energy fluxes, the larger the difference between the energy fluxes computed with the distribution and the corresponding mean. Entekhabi and Eagleason (1989) also stressed the importance of spatial variability of soil moisture and precipitation for the parameterization of land-surface processes.

Land-surface heterogeneity induces over domains within meso-γ scale preferent scales in the convective boundary layer. Such scales are characterized by organized rolls of size equivalent to length-scale of the surface heterogeneity (Baidya Roy and Avissar, 2000; Avissar and Schmidt, 1998). Also the heterogeneity linked to the topography affects soil moisture distribution. The acknowledgement of this effect allows a different land-surface modelling strategy based on the partitioning of the surface into a mosaic of hydrologic catchments, defined through analysis of high-resolution elevation data (Koster *et al.*, 2000; Ducharne *et al.*, 2000).

Giorgi (1997a, 1997b) represents the surface heterogeneity assuming that surface temperature and soil water content can be described by continuous analytical probability density functions (PDFs), and by integrating relevant non-linear terms over the appropriate PDF. His choice of linear symmetric PDFs allows analytical integrations which considerably reduce the computing time needed for this scheme. With the "statistical dynamical" approach (Avissar, 1992; Famiglietti and Wood, 1994; Sivapalan and Woods, 1995) surface inhomogeneities of vegetation and soil characteristics vary according to distributions that can be approximated by PDFs. Grid-scale average surface fluxes are explicitly calculated using numerical or analytical integration over appropriate PDFs. This approach, however, can be computationally demanding when several land characteristics need

to be represented by PDFs.

Effective (or aggregated) parameters are parameters which account for the non-linear effects explicitly calculated with the statistical dynamical approach. A few averaging techniques have already been proposed to compute effective parameters for land processes of atmospheric numerical models (*e.g.*, Noilhan and Lacarrere, 1995; Wood and Mason, 1991; Dolman and Blyth, 1997; Sellers *et al.*, 1997; Noilhan *et al.*, 1997; Kabat *et al.*, 1997, Rodriguez-Camino and Avissar, 1999). For instance, an effective surface roughness has been considered by André and Blondin (1986), Wieringa (1986), Taylor (1987), Mason (1988) and Claussen (1990, 1991) and an effective stomatal resistance was proposed by Claussen (1990) and by Blyth *et al.* (1993). However, Blyth *et al.* (1993) pointed out that parameter aggregation fails to represent strongly varying conditions. This is due to the non-linearity of the relationship between turbulent fluxes and vertical mean profiles. For instance, the vertical gradient of potential temperature can be positive on average over a large area, while local fluxes can be in opposite direction due to a local negative gradient of temperature, as explained, *e.g.*, by Stössel and Claussen (1993). The effects of soil moisture aggregation were estimated by Sellers *et al.* (1997) and Wood (1997). Finally, the impact of using effective land surface properties in atmospheric models at different scales has been studied among many others by Sellers *et al.* (1995) using the FIFE-89 data set, by Noilhan and Lacarrere (1995) using the HAPEX-MOBILHY-1986 data set and by Noilhan *et al.* (1997) using the EFEDA data set.

The so-called "mosaic of tiles" approach circumvents these problems by coupling independently each land-use patch or "tile" of a grid element to the atmosphere of the model, and patches affect each other only through the atmosphere. The primary motivation for the tiling approach is to promote suitable balance enhancements in horizontal complexity and to increase the physical realism of modelled surface energy and water fluxes. However, the main justification of the "mosaic of tiles" approach is the correctness of energy budget for each tile and, consequently, a better description of each fluxes. Comparisons of a grid-point model output against field data frequently face with the fact that observational sites are located over fairly homogeneous areas with only small variations in the gross vegetation type. Only a few surface field campaigns supply surface fluxes over more than one type of vegetation and therefore they are adequate to assess the benefits of a tiled model structure (see, *e.g.*, the comparison against BOREAS data described by Betts *et al.* (2001) and van den Hurk *et al.* (2000)). The "mosaic of tiles" approach was introduced by Avissar and Pielke (1989), and adopted by Claussen (1991), Koster and Suarez (1992) and Decoudré *et al.* (1993). The use of a tiled surface has also been recently incorporated to several operational NWP models (Bringfelt, 1996; Cox *et al.*, 1999; van den Hurk *et al.*, 2000).

Because the dependence of surface fluxes on land characteristics is non-linear, estimates of the area averaged fluxes calculated with mean land characteristics (effective parameters) do not yield the same results as those obtained by calculating the fluxes locally (as in the "mosaic of tiles" approach) and then averaging them (Li and Avissar, 1994). Thus, the choice of effective land characteristics, such as leaf area index or soil water content, is not straightforward.

2.2 Land surface parameterization schemes

The land-surface processes and their parameterization in NWP models are important for a number of reasons. The radiative solar and atmospheric fluxes absorbed by land-surface are mainly redistributed as latent and sensible heat. Both heat fluxes are the main mechanisms to turn back energy

into the atmosphere from land surface. Moreover, the sensible and latent heat fluxes at the surface are the lower boundary for the enthalpy and moisture equations in the atmosphere. The relative importance of sensible and latent heat fluxes depend strongly on surface features. In bare, dry soils, the absorbed radiative energy is mostly used to heat the surface, turning back the energy to the atmosphere usually as a vigorous, turbulent sensible flux. On the other hand, densely vegetated surfaces with enough water available for evapotranspiration invest most of the radiative energy in extracting subsurface water through the root system. The process of transpiration is mainly controlled by leaves, opening and closing their stomata according to the environmental conditions and to the available soil water. Transpiration turns energy back to the atmosphere in form of latent heat flux (Garrat, 1992; Viterbo, 1996). Land surface processes are also responsible of near surface weather parameters, such as screen level temperature and relative humidity, and low level cloudiness. Surface conditions provide also the appropriate feedback mechanisms for other physical processes in the atmosphere: low level cloudiness influences the surface radiative balance, sensible and latent heat fluxes influence the boundary layer structure and the triggering and intensity of convective processes. The partitioning of radiative energy between sensible and latent heat fluxes is related to the vegetation and soil properties, singularly to soil water availability. As mesoscale models continue to increase their spatial resolution, the density of the observation network is unable to capture the initial mesoscale structure at small scales. The majority of such mesoscale structures that are missed by the observation network are resulting from land surface forcing by topography, soil moisture, surface vegetation and soil characteristics. Therefore, it is crucial that mesoscale models include not only an advanced land surface model (LSM) but also a fine scale and realistic physiographic description of the land surface. The important role of the specification of initial conditions for soil water content has already been commented on.

Many investigations have already addressed the importance of the different land-surface parameters in atmospheric modelling (*e.g.*, Mintz, 1984; Walker and Rowntree, 1977; Rowntree and Bolton, 1993; Miyakoda and Strickler, 1981; Shukla and Mintz, 1982; Charney *et al.*, 1977; Chervin, 1978; Carson and Sangster, 1981; Sud *et al.*, 1988; Dickinson and Henderson-Sellers, 1988; Sud *et al.*, 1990; Henderson-Sellers, 1993, 1996a, 1996b, 1993c; Xue *et al.*, 1996). Collins and Avissar (1994) have first used the Fourier Amplitude Sensitivity Test (FAST) to estimate the relative importance of land-surface parameters. Rodriguez-Camino and Avissar (1998) have also estimated the most relevant land-surface parameters by comparing different land-surface schemes and using the FAST technique. This last study demonstrates that four parameters can explain most of the variance of surface heat fluxes under a broad range of environmental conditions. Soil wetness plays a predominant role for the heat fluxes. Roughness length is the most important parameter for the momentum flux. Leaf area index, in vegetated land, and texture, mainly in bare land, have also a significant impact on the fluxes. Roughness length is usually more important for sensible heat flux than for latent heat flux, and is mostly important under stable atmospheric conditions. Soil wetness and vegetation parameters are the dominant parameters under buoyant conditions.

Recent reviews of methods for representing land-surface processes in NWP and climate models include Garrat (1993), Schmugge and André (Eds., 1991), and Viterbo (1996). Land-surface schemes in NWP models have very much evolved from the so-called "bucket model" for estimating evaporation and runoff (Manabe, 1969). Deardorff (1978) introduced the use of restoring and forcing terms for both temperature and soil water content. At the same time he also introduced a foliage layer (or "big layer" model) to simulate the contribution of evapotranspiration from plants to the latent heat flux. In fact, most of the currently used schemes for NWP models (Dickinson *et al.*, 1993; Sellers *et al.*, 1986; Chen *et al.*, 1996; Noilhan and Planton, 1989) mimic the effect of plant physiology to regulate the opening and closing of leaf stomata. Stomata are sensitive to

certain environmental conditions (*i.e.*, solar radiation, temperature, humidity, carbon dioxide, and soil water potential in the root zone). The concept of stomatal resistance as a product of different functions was first intruced by Jarvis (1976) and it is common to most schemes.

As pointed out by Viterbo (1996), Richardson (1922), in his pioneer book on NWP, identified practically all relevant subjects in land surface parameterization. A quick summary of his work in this field is practically a description of the basic principles of current land surface schemes. First, he noticed that the formulation of lower boundary conditions for the atmospheric equations simplifies greatly if soil water content is also forecasted. He is probably the first to write an equation for the water transfer in the unsaturated part of the soil by generalizing the Darcy's law originally formulated for the flow of water in a saturated medium. He integrated the resulting partial differential equation with precipitation and evaporation as top boundary conditions. He also proposed to specify soil hydraulic properties depending on soil water content. For the heat transfer, he applied the classical Fourier law with heat conductivity depending on soil water content. The top boundary condition is the net heat flux at the surface. For the computation of evaporation from the canopy, he recognizes the physiological control of plants depending on soil moisture. He also made use of the concept of canopy resistance based on the electric analogy. Finally, he also used an interception reservoir, representing the leaves, able to collect precipitation and to evaporate at the potential rate.

Coupling a surface scheme in a NWP model involves several complex issues. First, the land-surface scheme should be relatively simple but at the same time it must be able to capture the essential features of the energy and hydrological fluxes. Second, the number of vegetation and soil parameters must remain within manageable limits, considering their relative impact on surface processes. Third, the physiographical description of soil and vegetation must be consistent with the complexity of the land surface scheme. Finally, the initialization of surface/soil variables (singularly of soil moisture) is a critical problem affecting the partition of surface energy and having implications on the model behaviour.

3 Analysis of surface variables

The use of land-surface parameterization schemes with increasing complexity implies the introduction of additional prognostic variables which in principle need to be initialized. Most land-surface schemes are based on simplifications of the equations for soil water transfer and for heat transfer. The prognostic variables introduced by these equations are usually soil water content and soil temperature. The major problem of specifying the initial conditions of these variables is the lack of routine observations. This is specially true in the case of soil water content. For soil temperature the climate network exists, but observations are not exchanged routinely via the GTS at the time of measurement. Consequently, in practice most stations performing observations at least daily can only be used, in delayed mode, for verification purposes. Another additional problem is the large spatial variability of soil water content and soil temperature, mainly inherited from the high heterogeneity of soil and vegetation properties. This large spatial variability associated with surface properties poses the added problem of using statistics of forecasts errors to spatially distribute the local increments. Such statistics are not known for soil variables.

The general problem of analysis of surface variables has been reviewed by Mahfouf and Viterbo

(1996). Description of different analysis techniques also applied for surface variables can be found in the classical text by Daley (1991). A review of measurement techniques of surface variables can be found in Schmugge and André (1991).

When considering time scales of a few days, soil water content variations appear to have a more significant influence on heat surface fluxes and on the planetary boundary layer than changes in other surface parameters, such as albedo, roughness length, etc. (see Rodriguez-Camino and Avissar, 1998). In fact, it has been shown that horizontal gradients of soil moisture can generate sea-breeze type mesoscale circulations (Ookouchy *et al.*, 1984) and can alter the location and intensity of severe storms (Lanicci *et al.*, 1987). It must be highlighted that the specification of initial conditions for soil water content affects model forecastings on all time scales: from short term to climate simulations (see *e.g.*, Garratt, 1993; Rowntree and Bolton, 1983; Rowell and Blondin, 1990; Yang *et al.*, 1994; Mahfouf, 1991).

Despite the sensitivity of short range forecasting to initial conditions of soil water content, few methods are currently available to estimate soil water in NWP models. The ground-based techniques include gravimetric method, neutron scattering, electromagnetic method, and tensiometer method. None of the above techniques is adequate for routine measurements due to a number of reasons: lack of representiveness of point measurements, excessive cost, human intervention needed, etc. The only feasible alternative is the use of satellite-based estimates of soil water content. Both infrared and microwave channels are informative about soil water content (see review in Schmugge and Becker, 1991). However, these estimates only provide information for the water content in the top few centimetres of the soil. No current satellite-based method of measurement can estimate soil water content in the root zone, as it is needed by most schemes. Some attemps have been made to retrieve soil water content in the root zone from surface water content and temperature estimates by inverting some land-surface scheme (Calvet *et al.*, 1998). Other authors have proposed soil water content estimates based on satellite computed heating rates (van den Hurk *et al.*, 1997). This last method, however, can only be applied for cloud-free pixels.

Two methodologies are currently applied in forecast/data assimilation systems for initializing soil water content. Mahfouf (1991) and Bouttier *et al.* (1993a, 1993b) proposed an optimal interpolation scheme (Daley, 1991) for the assimilation of soil water using the information of both temperature (T_{2m}) and relative humidity (RH_{2m}) at the heigth of two meters, which can be formally written:

$$W_a - W_f = \alpha^T (T_{2ma} - T_{2mf}) + \alpha^H (RH_{2ma} - RH_{2mf}) \tag{1}$$

The optimal interpolation coefficients α^T and α^H minimize the analysis variance and are related to the forecast error statistics. The subscripts a and f refer to the analyzed and forecast values, respectively. This method assumes a linear relationship between screen variable increments and soil moisture corrections, which is a rather crude approximation. Therefore, the major disadvantage of this method is that errors in screen variables that are not related to soil moisture effects will lead to soil moisture corrections. In reality, the signal in the bias of near-surface temperature and humidity is only related to soil water content under restricted synoptic conditions: small horizontal advection, no snow cover, absence of precipitation, daytime, etc.

Another alternative is the variational method, which seems more appropriate to treat the non-

linear dependence between screen variables and soil moisture and to assimilate measurements distributed in time. Mahfouf (1991), Hess (2000) and Balsamo *et al.* (2001) have used a 1D-Var approach to estimate the initial soil moisture best fitting to observations of temperature and relative humidity during a diurnal cycle. Therefore, the optimal soil water content minimizes the following cost-function:

$$J(W) = \sum_{i=1}^{N} \left[\left(\frac{T_{2moi} - T_{2mfi}}{\sigma_T} \right)^2 + \left(\frac{RH_{2moi} - RH_{2mfi}}{\sigma_{RH}} \right)^2 \right] \tag{2}$$

σ_T and σ_{RH} are the assumed observational errors of temperature and relative humidity, respectively, and the subscripts oi and fi represent the observation i and the forecast value interpolated to the point i. The summation goes over the total number of observation points, N.

The only existing method for initializing deep soil temperature consist of correcting soil temperature proportionally to the analysed increments of 2-metre temperature (Coiffier *et al.*, 1987). Optimal interpolation and variational approaches are in principle more adequate to initialize also deep soil temperatures.

Analyses of 2-metre temperature and relative humidity over land are needed, apart from their obvious relevance in diagnosis studies, to analyze soil water content based on screen variables increments (Mahfouf, 1991; Navascués, 1997). Both screen variables are analyzed from measurements in SYNOP reports. Screen variables show high heterogeneity inherited from surface properties: topography, vegetation, etc.

Snow covered surfaces deserve a special treatment as their features and physical mechanisms differ substantially from the snow free surfaces. First, the high snow albedo (close to 0.85 for recent snow) reduces substantially the available energy at the surface. Second, the snow layer acts as a insulator between the atmosphere and the soil. Third, the snow cover shows a high heterogeneity linked to the orography and to the vegetation type. The most simple models only add one equation for snow mass, which needs to be initialized. The snow mass analysis can benefit both from ground-based observations (snow-depth, snow fall) (see *e.g.*, Brasnett, 1999) and from microwave satellite imagery (see *e.g.*, Armstrong and Hardman, 1991; Hallikainen, 1996a, 1996b). Furthermore, satellite information helps to discriminate snow covered surfaces by their exceptionally high albedo.

Finally, some authors have recently shown that the specification of vegetation properties, such as vegetation cover, leaf area index (LAI), vegetation albedo, etc., and its right seasonal variation have a significant impact on near ground atmospheric variables (Champeaux *et al.*, 2000; Xue *et al.*, 1996). The use of land-use maps together with monthly varying correspondence tables for vegetation features is the most commonly accepted way to specify the slowly evolving fields describing vegetation properties. The use of satellite data able to capture vegetation indexes and their seasonality is the appropriate tool to estimate vegetation variables.

4 Selection of the land surface model

The importance of land surface processes in mesoscale modelling has been increasingly recognized over the last years (Bougeault *et al.*, 1991; Pielke *et al.*, 1997; Bringfelt *et al.*, 1999; Chen and Avissar, 1994a,b). In fact, mesoscale structures which are hardly captured by the observation network can only be produced during the model integration either by the atmospheric forcing or by the lower boundary forcing. The efforts to represent land-atmosphere processes in a realistic and accurate way have resulted in a rather big number of surface schemes with a wide variety of complexity. From the simplest ones based on the "bucket" concept (Manabe, 1969) up to the more complex models using a very comprehensive treatment of biophysical and radiative interaction between soil, vegetation and atmosphere (*e.g.*, Sellers *et al.*, 1986; Dickinson, 1993; Xue *et al.*, 1991), the range of intermediate possibilities is rather big.

The recent Project for Intercomparison of Land-Surface Parameterization Schemes (PILS) (Henderson-Sellers *et al.*, 1993; Henderson-Sellers *et al.*, 1995; Shao and Henderson-Sellers, 1996; Chen *et al.*, 1997; Wood *et al.*, 1998) has shown that even forcing with the same conditions, the simulated surface heat fluxes, soil moisture and runoff by different LSMs can vary between a wide range of values. Another surprising feature of the comparison is that sophisticated LSMs hardly outperform the relatively simple schemes. Among the reasons behind the modest results of the most complex models can be mentioned the following: (i) the big number of soil and vegetation parameters which usually are difficult to specify over all domains of integration; (ii) the excessive number of layers supplies in principle a better discretization of the heat and water transfer equations, but on the other hand increases the number of variables to analyse; (iii) lack of adequate physiographic data at the model resolution; (iv) absence of an appropriate treatment of the land surface heterogeneity present in the real world.

Taking into account the big number of existing schemes, the following list of desirable features was also considered: (i) the number of soil and vegetation parameters should be kept to a minimum; (ii) schemes should be well tested and validated both in field experiments and in operational environments; (iii) schemes should be able to simulate accurately the diurnal cycle of surface heat fluxes; (iv) incorporation of some solution for the initialization of the soil moisture and soil temperature fields; (v) existence of physiographic data consistent with model requirements.

The Interaction Soil-Biosphere-Atmosphere (ISBA) model meets all the requirements stated above and consequently was finally selected to simulate the land surface tiles. ISBA is a refinement of the Deardorff (1978) scheme. It makes use of the force-restore method for both temperature and soil water content. It consist of a thin layer (1 cm) reacting very quickly to the atmospheric forcing and a total layer (typically 1 m depth) where bulk water content is computed. The diurnal timescale forces the thermal equation, while for the water budget the forcing for each layer is parameterized based on the soil texture and the Clapp and Horberger (1978) relationships. It may be argued that the force-restore method is a rather crude approximation and that direct integration of the Fourier and Richards equations for heat and water transfer would be preferable. Dickinson (1988) has, however, demonstrated the theoretical equivalence of both methods.

The ISBA scheme makes use of a very limited number of surface parameters. In fact, the knowledge of the soil type (texture) and the vegetation type allows the computation of the hydraulic properties of the soil and the vegetation features affecting evapotranspiration, interception by the foliage and radiative effects.

ISBA has been successfully applied at single-point (Noilhan and Planton, 1989), mesoscale (Bougeault *et al.*, 1991) and global GCMs (Giard and Bazile, 2000). It has been validated against field experiment in a wide range of atmospheric conditions and ecosystems (see Noilhan and Mahfouf (1996) for a short review). ISBA or variants thereof is the scheme used in the following operational NWP models: ARPEGE/ALADIN (Giard and Bazile, 2000), ARPS (Xue *et al.*, 2001), HIRLAM (Bringfelt, 1996), GEM (Côté *et al.*, 1998).

Mahfouf (1991) studied the feasibility of soil moisture analysis from observations of 2-metre temperature (T_{2m}) and 2-metre relative humidity (RH_{2m}) using ISBA in 1D mode. Both variational and optimal interpolation (OI) methods were considered, and the corresponding statistics were derived using a Monte Carlo method for a discrete set of soil and vegetation features. Further steps with sequential OI analysis of surface and deep soil water contents using an analytical formulation for the OI coefficients were given by Bouttier *et al.* (1993a,b) and Giard and Bazile (2000), crystallizing in an algorithm well adapted to the vegetation and soil parameters used by the ISBA scheme.

Big efforts have also been pursued to improve the physiographic description of the surface with the same accuracy and horizontal resolution as the host NWP models using ISBA. Using Advanced Very High Resolution Radiometer (AVHRR) data from NOAA satellites, Champeaux *et al.* (2000) have designed a method based on an automatic clustering of multi-temporal Normalized Difference Vegetation Index (NDVI) maximum values to characterize eleven vegetation classes. Forest were previously identified from a thorough analysis of visible reflectances in early summer. The use of look-up tables assigning monthly values to the following ISBA vegetation parameters (roughness length, leaf area index, fractional vegetation cover and minimum stomatal resistance) allows to map them and aggregate them from the original 2 km resolution to the model resolution. The use of look-up tables assigning parameters to certain vegetation classes restrict the use of the physiographic description to a relatively small region of the globe (Europe in this case).

5 Brief description of the parameterization of surface processes

5.1 Treatment of heterogeneity

The HIRLAM surface scheme makes use of the *mosaic of tiles* or *aggregation of fluxes* approach mentioned above. Such approach represents the surface heterogeneity within one grid element assuming the existence of different land-use patches which evolve independently and couple directly to the atmosphere of the model. The land-use patches within one grid square affect each other only through the atmosphere.

In principle, the scheme may treat an arbitrary number of surface types in each grid square (Bringfelt, 1996). Several global and local physiographic databases were merged to assign a geographically–dominating vegetation type and soil texture for each subgrid surface. At present, five surface types are considered within each grid square: sea/lake water, ice, bare land, forest and agricultural terrain/low vegetation. However, the code maintains a high flexibility to allow easy implementation of more complex tiling approaches in the future if required.

At each time step, the sensible (H_i) and latent (E_i) heat fluxes from each subgrid surface are

weighted according to their fractional share of the grid square to form the total surface fluxes. The aggregated fluxes were used at the lowest model level as a lower boundary condition for the boundary layer vertical diffusion and the radiation schemes. At this level the wind, temperature and humidity were kept constant within the whole grid square. The surface fluxes H_i and E_i are based on the differences in temperature and humidity, between the lowest model level and the surface values for each sub-surface type, respectively. The atmospheric stability functions used for the computation of the aerodynamic resistance are given in Louis *et al.* (1982). The vegetation surface resistance for conditions, respectively. The vegetation surface resistance for transpiration includes the effect of the solar radiation, water stress in the root zone, water vapour deficit and air temperature, following Noilhan and Planton (1989). For the calculation of H_i and E_i the local roughness length due to vegetation is used.

The weighted momentum flux is calculated using a different strategy, mainly based on the computation of an effective roughness length. The momentum roughness length is obtained by adding the orographic roughness length, $z_{0_{orog}}$, and an aggregated local vegetation roughness length ($z_{0_{veg}}$), which in turn is computed by averaging from the local roughness lengths for the subsurfaces (z_{0_i}) according to Mason (1988): $1/(ln\frac{l_b}{z_{0_{veg}}})^2 = \sum f_i/(ln\frac{l_b}{z_{0_i}})^2$, where l_b is the blending height or the height at which the flow becomes approximately independent of horizontal position (Claussen, 1991). The main justification of the parameter aggregation for the momentum roughness length resides in the different behaviour of the momentum and heat transports. The momentum exchange is disproportionally affected by the large roughness elements in the domain (Blyth *et al.*, 1993; Dolman and Blyth, 1997), whereas the effective roughness length for heat is dominated by the smooth elements with low values of the roughness length (Wood and Mason, 1991). Also the no-slip condition at the surface (implying that the velocity is always zero) affects in the same way the contribution of different elements within a grid square to the momentum exchange. In contrast, transport of heat lacks a no-slip condition at the surface and the calculation of an effective resistance to heat transport is complicated by the variability in surface temperature. The usage of different averaging (aggregation) procedures for heat/moisture and momentum is not a novelty and it has already been proposed by several authors (*e.g.*, , Dolman, 1993; Blyth *et al.*, 1993).

In reality, the blending height, above which the structure of turbulence has attained horizontal homogeneity by turbulent mixing, is expected to vary with the patchiness and the mixing activity (*i.e.*, essentially stability). Assuming that the blending height is of the order of 1/100 of the horizontal scale of the roughness variations (Claussen, 1995)), for typical landscape variations of 1000 m the blending height is of the order of 10 m. For our computation purposes, a constant blending height ($l_b = 10.$) has been used. This choice certainly imposes restrictions to the lowest model level, which should be higher than l_b. The time step should be accordingly chosen in order to allow the turbulent mixing to reach horizontal homogeneity at the blending height. However, cases of high blending heights can sporadically occur, as *e.g.*, in convective situations, and it may happen that the lowest model layer violates the assumption of one single value for all fractions. This is probably not too serious and for most of the cases can be assumed that the lowest model level is above the blending height.

Diagnostic fields, such as 2-metre temperature and relative humidity, 10-metre wind, etc., are also computed and are available for each grid box fraction separately.

For sea/lake, there is no energy balance equation for calculating the water temperature: this quantity is kept constant. The surface roughness of the water is calculated using the modifications

to the Charnock (1955) formula proposed by Nielsen (1999) for the smooth surface regime. For ice, a three layer model for temperature is used based on the one-dimensional equation for vertical heat diffusion with constant heat capacity and diffusivity in time and space (Källen, 1996).

The current formulation of the surface scheme here described does not include specific tiles for snow covered surfaces. Given the importance of a separate energy balance equation for high and low vegetation tiles with snow, work is on progress to add the corresponding tiles (S. Gollvik, personal communication).

The surface analysis part is consistent with the tiled structure used in the parameterization part. In particular, only one analysis of 2-metre temperature and relative humidity is conducted for the averaged of the three land subtypes. It is worthwhile to note that the average surface specific humidity includes the contributions from both the canopy evapotranspitation and the ground evaporation.

5.2 The ISBA land surface scheme

A brief description of the variables and equations in the ISBA scheme is provided here. The algorithm described in the original paper (Noilhan and Planton, 1989) has been upgraded with a number of additions and modifications (see (Noilhan and Mahfouf, 1996) and (Giard and Bazile, 2000) for the most updated versions of the scheme and (Bringfelt, 1996) for the first HIRLAM implementation.

5.2.1 Equations of the scheme

The prognostic equations for the surface temperature, T_s, and for its mean value, T_2, over one day, τ, are obtained from the force-restore method. The surface temperature is representative of the soil-vegetation medium. The corresponding equations are:

$$\frac{\partial T_s}{\partial t} = C_t G - \frac{2\pi}{\tau}(T_s - T_2) \tag{3}$$

$$\frac{\partial T_2}{\partial t} = \frac{T_s - T_2}{\tau} \tag{4}$$

where G is the sum of the fluxes at the surface in the soil-vegetation medium (net radiation flux (R_n), sensible heat flux (H) and latent heat flux ($L_v E$)) and C_t is the thermal coefficient expressed by

$$C_t = \left[(\frac{1 - veg}{C_g} + \frac{veg}{C_v}) \right]^{-1} \tag{5}$$

here veg is the fraction of vegetation, C_v is the thermal inertia coefficient for the canopy, which has been tuned to $8 \times 10^{-6} Km^2 J^{-1}$, and C_g is the thermal inertia coefficient for the soil, which adopts the following expression (Giard and Bazile, 2000):

$$C_g = min \left\{ C_{g_{max}}, C_{g_{sat}} \left[\frac{w_{sat}}{max(w_2, w_{wilt})} \right]^{(b/log10)} \right\} \tag{6}$$

here, b is the slope of the retention curve and $C_{g_{sat}}$ is the soil thermal coefficient at saturation. Both are estimated for each soil texture (Noilhan and Planton, 1989). C_g is limited to its value at wilting point, with a maximum $C_{g_{max}}$ set to $8 \times 10^{-6} Km^2 J^{-1}$. These limits are imposed for a better representation of the diurnal cycle of surface and low-level atmospheric variables. This constraint may be revised later with further improvements in the rest of the physics.

For the treatment of the soil water, an analogous force-restore model has also been applied. The soil is divided, as it was already mentioned in Section 4, in two layers: one surface layer (d_1), with a depth typically of 1 cm, interacting directly with the atmosphere, and a total soil column (d_2) extending down to a depth of about 1 m. The prognostic equations for the surface, w_s, and total, w_2, volumetric water content are defined in the corresponding layers. Over the vegetation a skin reservoir for the rain (dew) water retained on the vegetation canopy, w_r. is defined. The corresponding equations are:

$$\frac{\partial w_s}{\partial t} = \frac{C_1}{\rho_w d_1}(P_g - E_g) - \frac{C_2}{\tau}(w_s - w_{geq}) \tag{7}$$

$$\frac{\partial w_2}{\partial t} = \frac{1}{\rho_w d_2}(P_g - E_g - E_{tr}) - \frac{C_3}{\tau} max[0, (w_2 - w_{fc})] \tag{8}$$

$$\frac{\partial w_r}{\partial t} = veg \cdot P - E_r, \; w_r \leq w_{rmax} \tag{9}$$

where ρ_w is water density, P_g is the precipitation reaching the soil, P is the precipitation at the top of the vegetation, E_g is the evaporation rate from the ground, which dries the shallow layer only, E_{tr} is the canopy transpiration flux from vegetation, which acts through the plant roots, E_r is the evaporation flux from the fraction δ of the foliage covered by intercepted water and w_{rmax} is the threshold value of the interception reservoir.

The hydric coefficient C_1 includes the idea of Braud *et al.* (1993) for dry soils further modified by Giordani (1993) and Giard and Bazile (2000):

$$C_1 = \begin{cases} C_{1max} d_1 exp[-(w_s - w_{max})^2/\sigma] & \text{for } w_s < w_{wilt} \\ C_{1sat} d_1 (w_{sat}/w_s)^{(b/2+1)} & \text{for } w_s \geq w_{wilt} \end{cases} \tag{10}$$

where C_{1max}, w_{max} and σ are the maximum, the abscissa of the maximum and the standard deviation of the Gaussian, respectively. w_{sat} is the saturated volumetric soil water content, which

depends on soil texture. C_{1max}, w_{max} and σ depend on the wilting point and surface temperature. The position (w_{max}) and width (σ) of the Gaussian curve are adjusted to ensure continuity of the formulation at the wilting point and to fix a minimum value for very dry soils: $C_1(0) = 0.1$.

The hydric restore coefficient C_2, characterizing the velocity at which the water profile is restored to its equilibrium, follows the original (Noilhan and Planton, 1989) formulation:

$$C_2 = C_{2ref}\left(\frac{w_2}{w_{sat} - w_2 + w_l}\right) \tag{11}$$

where w_l is a small numerical value preventing any singularity at the saturation point. The coefficient C_{2ref} has been estimated for different soil textures.

The drainage coefficient C_3 is a relaxation coefficient of total water content to the field capacity (w_{fc}), to simulate the gravitational drainage. It depends only on soil texture (Mahfouf *et al.*, 1994)

The equilibrium surface water content w_{geq} (when gravity balances capillarity forces) is used instead of the total water content for the restore term. It follows the original formulation:

$$w_{geq} = w_{sat}\left[\frac{w_2}{w_{sat}} - a\left(\frac{w_2}{w_{sat}}\right)^p\left(1 - \left(\frac{w_2}{w_{sat}}\right)^{8p}\right)\right] \tag{12}$$

The parameters a and p have been estimated for different soil textures.

5.2.2 Surface fluxes over land

The turbulent latent and sensible heat fluxes are computed using the classical aerodynamic expressions. For the sensible heat flux:

$$H = \rho_N c_p C_H V_N (T_s - T_N) \tag{13}$$

where c_p is the specific heat, and T_N, V_N and ρ_N are the temperature, the wind speed and the air density at the lowest model level, respectively. C_H is the drag coefficient depending on the thermal stability of the atmosphere. It is computed using the atmospheric stability functions given in Louis *et al.* (1982).

The latent heat flux, L_vE, formulation closely follows Noilhan and Planton (1989). It includes the evaporation, E_g, from the ground and the evapotranspiration, E_v from the vegetation:

$$E_g = (1 - veg)\rho_N C_H V_N (h_u q_{sat}(T_s) - q_N) \tag{14}$$

$$E_v = veg\,\rho_N C_H V_N h_v (q_{sat}(T_s) - q_N) \tag{15}$$

where $q_{sat}(T_s)$ is the saturated specific humidity at temperature T_s, and q_N the atmospheric specific humidity at the lowest model level.

The relative humidity at the ground surface, h_u, is related to the surface soil moisture, w_g, through the following expression:

$$h_u = \begin{cases} \frac{1}{2}[1 - cos(\frac{w_g}{w_{sat}}\pi)], & \text{if } w_g < w_{sat} \\ 1, & \text{if } w_g \geq w_{sat} \end{cases} \tag{16}$$

When the evapotranspiration flux, E_v, is positive (upwards), the Halstead coefficient, h_v, takes into account the direct evaporation, E_r, from the fraction, δ, of the foliage covered by intercepted water, as well as the transpiration, E_{tr}, of the remaining part of the leaves. When E_v is negative, the dew deposition is supposed to take place at the potential rate ($h_v = 1$).

$$\begin{aligned} h_v = &\quad (1-\delta)R_a/(R_a+R_s) + \delta \\ E_r = &\quad veg\frac{\delta}{R_a}\rho_N(q_{sat}(T_s) - q_N) \\ E_{tr} = &\quad veg\frac{1-\delta}{R_a+R_s}\rho_N(q_{sat}(T_s) - q_N) \end{aligned} \tag{17}$$

where $\delta = (w_r/w_{rmax})^{2/3}$ (Deardorff, 1978) and the aerodynamic resistance, R_a, is equal to $1/(C_H V_N)$.

The surface resistance, R_s is expressed by the product of a minimum resistance, R_{smin}, and a number of limiting factors (Jarvis, 1976) depending on environmental conditions (radiation, water stress, water vapor deficit and air temperature):

$$R_s = \frac{R_{smin}}{LAI} {F_1}{F_2}^{-1}{F_3}^{-1}{F_4}^{-4} \tag{18}$$

The factor F_1 measures the influence of the photosynthetically active radiation, PAR, (Sellers, 1985) which is assumed to be equal to $0.55(1-\alpha)R_g$:

$$ {F_1}^{-1} = 1 - a_1 log\frac{a_2 + PAR}{a_3 + PAR} \tag{19}$$

where R_g is the incoming solar radiation, α is the vegetation albedo, and a_1, a_2 and a_3 are parameters depending on canopy properties (see Sellers, 1985) which are assigned the values proposed by Blondin (1991): $a_1 = 0.19$, $a_2 = 1128 W m^{-2}$ and $a_3 = 30.8 W m^{-2}$. This formulation of the factor F_1 gives a smoother dependency on PAR than the original one in Noilhan and Planton (1989), which for certain combinations of canopy properties show a very strong sensitivity to small variations of PAR.

The factor F_2 takes into account the effect of water stress on surface resistance:

$$F_2 = \begin{cases} 1 & \text{if} \quad w_2 > w_{fc} \\ \frac{w_2 - w_{wilt}}{w_{fc} - w_{wilt}} & \text{if} \quad w_{wilt} \leq w_2 \leq w_{fc} \\ 0 & \text{if} \quad w_2 < w_{wilt} \end{cases} \tag{20}$$

where w_{fc} and w_{wilt} are field capacity and wilting point, respectively.

The factor F_3 represents the effects of vapor pressure deficit of the atmosphere:

$$F_3 = 1 - g(q_{sat}(T_N) - q_N) \tag{21}$$

where g is only different from zero in case of coniferous forests ($g = 40$)

The factor F_4 introduces an air temperature dependence on the surface resistance (Dickinson, 1993):

$$F_4 = 1 - 0.0016(298 - T_N)^2 \tag{22}$$

The phase changes of water in the soil may have an important effect on the water and energy transfer in the soil. The freezing and thawing of soil water manifest as a "thermal barrier" at about 0^oC, making soil temperatures less responsive to the atmospheric forcing. Therefore, the main impact will be both to delay the soil cooling when dropping temperatures and to delay the soil warming in spring when the solar forcing starts to melt frozen surfaces. The flux due to the soil water change of phase (F_i) can be expressed by:

$$L_i \rho_w (1 - veg) d_2 \partial w_i / \partial t \tag{23}$$

where L_i is the latent heat of fusion and $\partial w_i / \partial t$ is the variation of the total ice water content. Following the ideas of Viterbo *et al.* (1999), the total ice water content can be assumed to be $w_i = f(T_s) w_2$, where $f(T_s)$ is a function taking the value 1 for temperatures well below 0^oC (all soil water content is in solid phase), 0 for temperatures well above 0^oC (all soil water content is in liquid phase) and with some smooth transition around 0^oC. To avoid undesirable coupling between the temperature and water equations w_2 is additionally assumed to be equal to the field capacity value, w_{fc}, in the expression for F_i. The final expression for the flux due to the soil water change of phase is:

$$F_i = [L_i \rho_w (1 - veg) d_2 w_{fc} df(T_s)/dT_s] \partial T_s / \partial t \tag{24}$$

This term has been included in the left-hand side term of the surface temperature equation and incorporates the barrier effect through the pulse-like function of surface temperature, $df(T_s)/dT_s$, to simulate the soil water content freezing/thawing around 0^oC.

The 'thermal barrier" method mimics the effect of reduced responsiveness of soil temperature to the atmospheric forcing due to the phase changes of soil water. It was originally designed for its use with a diffusion equation for soil temperature. Its application to the force- restore scheme described here implies some additional retuning which is currently under way.

Snow sub-fractions are allowed within the ice fraction and within each of the land-surface fractions. Snow is represented by a single layer with a prognostic equation for snow depth. Two options are additionally available for the snow treatment: one modifying the thermal coefficient and albedo over snow covered fractions, and another including additional equations for snow density and snow albedo to simulate the ageing process of the snow (Douville *et al.*, 1995). The snow parameterization is complemented in both options with a 6 hourly snow depth analysis based on a successive correction method making use of observations.

6 Description of the surface analysis algorithm

The HIRLAM surface analysis is consistent with the mosaic approach adopted in the parameterization of soil/surface processes. As it has already been documented above, five different tiles are allowed within each grid square: water, ice, bare ground, low vegetation, and forest. The surface analysis module has been developed from the original surface parameter analysis operational at SMHI (Gustafsson, 1985) and the assimilation of soil water content based on the sequential method (Bouttier *et al.*, 1993a, 1993b; Giard and Bazile, 2000) It has been substantially modified to adapt it to the current parameterization requirements. It provides initial values to the following variables: water surface temperature (SST), fractions of ice and water, snow depth over ice and land fractions, screen level temperature and relative humidity over land fractions, superficial and mean soil temperatures, and superficial and total volumetric water contents.

6.1 Analysis of water surface temperature

As it has already been described in Subsection 5.1, both sea and lake water are considered one of the five types of surface within a grid square. It was also mentioned that water temperature is kept constant during the integration. Consequently, the water surface temperature is only updated during the assimilation step. The analysis of surface temperature, contrary to the surface parameterization, provides a separate treatment to the inland lake and sea water fractions.

At each assimilation step, a background field is generated by relaxing the previous analysis to the corresponding climatological field. This relaxation ensures a correct seasonal evolution over persistently data void areas. Sea surface reports (SHIP and BUOY) and pseudo-observations generated from the ECMWF sea surface temperature field (produced daily by NCEP) provide an uniform density of data over open ocean. Special observations, as *e.g.*, locally derived SST values from AVHRR radiances, can be added optionally.

The observation operator consists of a bi-linear interpolation. It takes additionally into account the type of surface, either open ocean or inland lakes, of both grid points and observation station. They can be classified into five different classes according to their fractions of land and lake: lake, inland, near coast, coastal and open sea:

Table 1: Classification of observation stations and grid points.

inland	near coast	coast	lake	open sea
$f_{land} > 0.8$	$0.8 \geq f_{land} > 0.5$	$0.5 \geq f_{land} > 0.2$	$f_{lake} > 0.02$	$f_{land} \leq 0.2$

Restrictions are imposed in the model interpolation of water surface temperature to the observations positions. Only grid points of similar type to the observation can be used to create the model equivalent of observed temperature. The only quality control to the data is a simple first guess check (each observed temperature should not be too different from the temperature in the previous analysis). The default analysis method is successive corrections. The formulation of a priori determined observations weights follows Cressman (1959):

$$w(r) = \begin{cases} \frac{R^2 - r^2}{R^2 + r^2} & r \leq R \\ 0 & r > R \end{cases} \tag{25}$$

Three iterations with successive radius R at 600 km, 400 km, and 150 km are applied.

In the current tiling scheme, water temperature and ice fraction represent two different fields. Their values over land and sea points refer to lakes and ocean, respectively. Thus, topography induces a discontinuity basically along the coast line, that should be taken into account. In particular, it is undesirable that a sea observation could influence surface temperature over lakes in the proximity (Eerola,1995). In order to account for this land-sea anisotropy, observations weights depend not only on horizontal distance but they are further scaled using the grid points and observation classification. The following table is used for the scaling factors, $f(class_i, class_k)$, considering the topographic features:

Table 2: Scaling factors associated to land/water anisotropy.

obs.class	grid point class				
	inland	near coast	coast	lake	open sea
inland	1.	0.5	0.0	1.	0.0
near coast	0.5	1.	0.5	0.5	0.3
coast	0.0	0.5	1.0	0.0	0.9
lake	1.	0.5	0.0	1.	0.0
open sea	0.0	0.3	0.9	0.0	1.0

The analysis at grid point k, at iteration $j+1$, a_k^{j+1}, is then

$$a_k^{j+1} = a_k^j + \frac{\sum_{i=1}^{N} W_{ik} \sigma_o^{-2} (y_i - a_i^j)}{\sum_{i=1}^{N} W_{ik} \sigma_o^{-2} + \sigma_b^{-2}} \tag{26}$$

where $y_i - a_i^j$ is the background departure at the i observation position, σ_o and σ_b are the observation and background error standard deviations, respectively, and W_{ik} are the weights given to

observations i=1,N:

$$W_{ik} = w(r_{ik}) f(class_i, class_k) \tag{27}$$

In the first iteration, a_i^j is the background field obtained by relaxing the previous analysis to the climatology.

Once that surface temperature over water has been analysed, fractions of water and ice are diagnosed. The algorithm is linear between two limiting temperature values. Different pairs of threshold values are used over the Baltic Sea, lakes and open ocean to take into account the water salinity.

6.2 Analysis of snow depth

The mosaic scheme allows snow mass accumulation in sea-ice and land fractions. Consequently, the analysed field is the fractional average over these tiles. The background snow mass is additionally relaxed to climatology and converted into snow depth by assuming a monthly varying snow density. The corresponding conversion factors (from water equivalent (m) to snow depth (cm)) are the following:

Table 3: Conversion factor from snow mass (m) to snow depth (cm)

Jan.	Feb.	Mar.	Apr.	May	Jun.	Jul.	Aug.	Sep.	Oct.	Nov.	Dec.
450	430	416	360	320	320	320	700	700	620	550	470

The only information used are the observations contained in land surface reports. The observation operator is simply a bi-linear interpolation. Data checking consists only of a first guess check. The analysis method is successive corrections with Cressman type dependence on horizontal distance of observation weights.

Observation weights are also vertically scaled to account for the difference between model orography and observation height and to prevent from getting analysed snow cover in the mountain surroundings in case of no availability of stations not reporting snow depth (Eerola, 1995). The scaling factor, $f(\Delta z)$, is

$$f(\Delta z) = \begin{cases} 0.0 & \Delta z \leq 0 \quad \mid \Delta z \mid \geq z_{crit} \\ \frac{{z_{crit}}^2 - \Delta z^2}{{z_{crit}}^2 + \Delta z^2} & \Delta z \leq 0 \quad \mid \Delta z \mid < z_{crit} \\ 1. & \Delta z > 0 \end{cases} \tag{28}$$

$$\Delta z = z^{mod} - z^{obs}$$

$$z_{crit} = 300m$$

The observation weights, $W_{ik}(r, \Delta z)$, are finally:

$$W_{ik}(r, \Delta z) = \begin{cases} f(\Delta z) \frac{R^2 - r^2}{R^2 + r^2} & r \leq R \\ 0 & r > R \end{cases} \tag{29}$$

Four scans are conducted at horizontal radius (R) 600 km, 400 km, 150 km and 100 km.

The analysed field converted back to equivalent water snow mass is copied into the ice and three land subtypes of surface.

6.3 Analysis of 2-metre temperature and relative humidity

Analysis of screen level variables is a useful tool for model validation or diagnostic studies. However, the main purpose here is to assimilate soil temperatures and water content at each land tile. Relative humidity is the chosen humidity variable to be analyzed, due to the easier modelling of first guess error statistics. Data used are 2-metre temperature and relative humidity (derived from dew point temperature) from SYNOP reports. The model state projection onto observation space is described in Navascues (1997). The projection operator consists of the following steps:

- Horizontal bi-linear interpolation to observation position of atmospheric vertical profiles. Only grid points with not negligible fraction of land are used.
- Vertical interpolation of the whole profile from the model orography to the station height. The algorithm preserves the stability structure in the boundary layer (Källen, 1996).
- Averaging of surface variables over land fractions: surface temperature and specific humidity, snow mass, and roughness length.
- Re-calculation of the surface temperature to keep the potential temperature lapse rate in the surface layer.
- Diagnosis of 2-metre temperature and relative humidity following Geleyn (1988).

An effective local roughness length, z_0, is created from the local roughness length at each land tile, $z_{0,i}$, by means of a blending height, z_b, following the method proposed by Mason (1988) and used in the diagnosis of near surface parameters:

$$\frac{1}{ln^2\left(\frac{z_b}{z_0}\right)} = \sum_i \frac{A_i}{ln^2\left(\frac{z_b}{z_{0,i}}\right)} \tag{30}$$

The analysis method for both near surface parameters is univariate statistical interpolation. It allows an additional quality control to data by checking each observation against its neighbours. This optimum interpolation check is only applied to active data, *i.e.*, data not rejected after the first guess check.

The autocorrelation model ρ is anisotropic, based on the relevant orographic features found when studying T_{2m} and RH_{2m} errors covariances corresponding to the old surface parametrization. The analytical formulation of the structure function consists of a gaussian dependence on both the horizontal and vertical distances $r, \Delta z$. Characteristic length scales have been set *ad hoc* as follows:

$$\rho(r, \Delta z) = exp[-0.5(\frac{r^2}{R^2} + \frac{\Delta z^2}{H^2})] \tag{31}$$

with $R = 100km$ for T_{2m}, $R = 75km$ for RH_{2m} and $H = 400m$ for both T_{2m} and RH_{2m}.

Preliminary values for observation and background error variances have been assigned after some experimentation. Both the ratio of observations to first guess errors and characteristic length scales have been tuned to avoid too noisy analysis increments, to minimize the rejected observations during the optimum interpolation check and to produce an analysis close to the observations.

The optimum interpolation check is performed by dividing the model area in boxes. Observations in a radius from the center of box are used together to decide the final status of data contained in the box. All active observations are afterwards used in wider analysis boxes to solve the analysis problem.

6.4 Analysis of soil temperatures

Surface, T_s, and mean layer, T_d, soil temperatures are separately analysed for each subtype of surface following Giard and Bazile (2000). The method is a simple correction based on the calculated 2-metre temperature analysis increment at every assimilation step:

$$\Delta T_d = \Delta T_{2m}/(2\pi) \tag{32}$$

$$\Delta T_s = \Delta T_{2m} \tag{33}$$

6.5 Analysis of soil water content

Surface, w_s, and total layer, w_d, water contents, are assimilated separately at each tile. Water intercepted by vegetation, w_r, is not analysed, being simply copied from the first guess to the analysis. The method to initialize w_s and w_d is based on the sequential assimilation developed by Mahfouf (1991), with optimum coefficients approximated analytically by Bouttier *et al.* (1993a,b), and totally rewritten for operational implementation in the ARPEGE model by Giard and Bazile (2000). It was implemented in HIRLAM by Ayuso (1995) simultaneously to the tiled surface package.

The analysed 2-metre temperature and relative humidity at each grid point are used as observations for the analysis of soil water contents. Soil moisture corrections are linearly calculated from the screen level analysis increments by means of an optimum interpolation analysis:

$$\Delta w_s = \alpha_s^T \Delta T_{2m} + \alpha_s^H \Delta H_{2m} \tag{34}$$

$$\Delta w_d = \alpha_d^T \Delta T_{2m} + \alpha_d^H \Delta H_{2m} \tag{35}$$

where $\alpha_s^T, \alpha_s^H, \alpha_d^T, \alpha_d^H$ are the optimum coefficients that minimize the mean square error of the estimation.

The statistics of the forecast errors on soil moisture was estimated by Mahfouf (1991). He used a Monte Carlo method consisting of a set of 24h perturbed one-dimensional simulations, each of them

started from a randomly modified soil moisture. Bouttier *et al.* (1993) analysed the distribution of the forecast errors statistics at each local solar time due to the variation of the incident radiation on the surface and the dependence of optimum coefficients on the surface characteristics. Then, they proposed an analytical formulation for $\alpha_s^T, \alpha_s^H, \alpha_d^T, \alpha_d^H$. The formulation of optimum coefficients in the current version differs from the original by Bouttier *et al.* (1993), and follows Giard and Bazile (2000). Coefficients depend on vegetation coverage, *veg*, local solar time, t^*, leaf area index, LAI, minimum stomatal resistance, R_{smin} and soil texture, *txt*:

$$\alpha_s^T = f(txt)(1-veg)\left[a_0^T(t^*) + a_1^T(t^*)veg + a_2^T(t^*)veg^2\right] \quad (36)$$

$$\alpha_s^H = f(txt)(1-veg)\left[a_0^H(t^*) + a_1^H(t^*)veg + a_2^H(t^*)veg^2\right] \quad (37)$$

$$\alpha_d^T = f(txt)\left\{(1-veg)\left[b_0^T(t^*) + b_1^T(t^*)veg + b_2^T(t^*)veg^2\right] + veg\frac{LAI}{R_{smin}}\left[c_0^T(t^*) + c_1^T(t^*)veg\right]\right\} \quad (38)$$

$$\alpha_d^H = f(txt)\left\{(1-veg)\left[b_0^H(t^*) + b_1^H(t^*)veg + b_2^H(t^*)veg^2\right] + veg\frac{LAI}{R_{smin}}\left[c_0^H(t^*) + c_1^H(t^*)veg\right]\right\} \quad (39)$$

Where $f(txt)$ accounts for the scaling of optimum coefficients for the different range of variation between wilting point, w_{wilt}, and field capacity, w_{fc}, for the different soil textures:

$$f(txt) = \frac{(w_{fc} - w_{wilt})_{txt}}{(w_{fc} - w_{wilt})_{loam}} \quad (40)$$

The coefficients in the polynomial terms, $a_i^T, a_i^H, b_i^T, b_i^H, c_i^T, c_i^H$, have been tuned by Giard and Bazile (2000), by fitting the adopted analytical function of the vegetation properties and local solar time to the original set of O.I. coefficients obtained by Mahfouf (1991).

A few constraints have additionally been imposed to prevent undesired corrections in synoptic situations such that the atmosphere is not sensitive to errors in soil moisture. Consequently, corrections to soil water content are not applied in the cases of snow covered surface, strong wind speed, significant rain, attenuation of solar radiation by clouds, very short length of daylight or dew deposition. Most of these conditions have been analytically introduced by means of scaling factors w_1, w_2, w_3, decreasing smoothly the soil moisture corrections following the ARPEGE model operational implementation (E. Bazile, personal communication):

$$w_1 = \begin{cases} \dfrac{\text{day length}}{\text{minimum day length}} & \text{day length} \leq \text{minimum day length} \\ 1 & \text{day length} > \text{minimum day length} \end{cases} \quad (41)$$

where the minimum day length is 6 hours.

$$w_2 = \begin{cases} 1. - \frac{\|\mathbf{v}^{10}\|}{\|\mathbf{v}^{10}_{max}\|} & \| \mathbf{v}^{10} \| \leq \| \mathbf{v}^{10}_{max} \| \\ 0. & \| \mathbf{v}^{10} \| > \| \mathbf{v}^{10}_{max} \| \end{cases} \quad (42)$$

where $\| \mathbf{v}^{10}_{max} \| = 10 ms^{-1}$.

$$w_3 = \begin{cases} 1. - \frac{prec}{prec_{crit}} & prec \leq prec_{crit} \\ 0. & prec > prec_{crit} \end{cases} \tag{43}$$

where the critical value of accumulated precipitation over the past 6 hours, $prec_{crit}$, has been set to 6 mm.

An analogous reduction of soil moisture increments in cloudy situations is modulated by the factor w_4:

$$w_4 = \begin{cases} 1. - \frac{cloud}{cloud_{crit}} & cloud \leq cloud_{crit} \\ 0. & cloud > cloud_{crit} \end{cases} \tag{44}$$

where $\text{cloud}_{crit} = 0.8$.

A further condition requires that soil moisture is only corrected provided that T_{2m} and RH_{2m} analysis increments have opposite signs.

The assimilation only takes place between wilting point and field capacity to avoid unrealistic corrections to the surface variables, provided that only within this range soil moisture is controlling the evaporation rate. In practice the lowest limit is set to veg*wilting point, to leave the minimum value allowed to have a dependence on the vegetation coverage.

The mean volumetric soil water content is changed by the mean of the last four analysis increments with the aid of a history file of soil wetness increments. It produces a smoother evolution of the soil moisture, as physically expected.

Systematic errors in screen level relative humidity are very much affected by errors in the specification of soil water content. However, 2-metre temperature systematic errors are very often due to other different reasons, as *e.g.*, errors in the radiative forcing. Following Giard and Bazile (2000), a systematic long-term T_{2m} increment, ΔT_{2f}^n is calculated at the n^{th} assimilation cycle:

$$\Delta T_{2f}^n = (1 - r)\Delta T_{2f}^{n-1} + r\Delta T_{2m} \tag{45}$$

with $r = 0.5$.

Instead of the full 2-metre temperature increment, obtained in the n^{th} screen level parameters analysis, ΔT_{2m}, only the T_{2m} effective increment, ΔT_{2m}^{eff}, defined as the deviation from this mean value is used to modify the soil moisture:

$$\Delta T_{2m}^{eff} = \Delta T_{2m} - \Delta T_{2f}^n \tag{46}$$

The above soil moisture corrections masking is based on a sequence of conditions, which identifies the lack of atmospheric sensitivity to the variation of soil water content. An alternative option could consist of a careful selection of the observations used in the analyses of 2-metre temperature and relative humidity. If similar conditions to the constraints (41)-(44) were applied to screen 2-metre observations, the subsequent analysis increments would no longer need of a masking procedure during the soil moisture assimilation step. However, it is very likely than then the insufficient number of observations and the simplicity of the hypothesis assumed for the formulation of the structure function would not be able to produce the appropriate analysis increments patterns in some areas, as *e.g.*, in the inland to coast direction. Furthermore, the 2-metre temperature analysis

plays an important role leading the time evolution of soil temperature in winter time. In any case, the screen level analyses are also a very useful tool to monitor the model performance and they also serve as input for many other operational applications, which otherwise would not be covered in some areas and for long periods (*e.g.*, snow covered regions).

7 Relevance of postprocessing and verification

The tiling approach to the parameterization of surface processes involves forecasting of surface variables for each of the tiles existing within a grid square. In the current approach each tile is fully independent from its neighbour tiles. Both surface and total (deep) layers do not have any coupling with any other tiles within the grid box. The only interaction between tiles in the same grid box takes place only through the lowest model layer. The added complexity of the tiled surface structure allows many different possibilities for postprocessing fields and also for verifying them against observations.

Diagnosed screen variables (2-metre temperature, 2-metre relative humidity, 10-metre wind) are computed for each existing tile within a grid square. Also the areal average value representative of the grid square is computed during the postprocessing. The ideal verification should proceed by comparing the observed value against the model equivalent to the observed variable. This process is routinely done during the assimilation step by comparing observations against the output from the analysis observation operator. In case of 2-metre temperature and relative humidity, the observation operator, first, interpolates horizontally and vertically the atmospheric profiles from model orography to station height, second, surface variables over land fractions are horizontally interpolated, third, surface temperature is re-calculated to keep stability structure in the surface layer and, finally, 2-metre temperature and relative humidity are diagnosed based on Geleyn (1988).

Some experimentation has proved that two of the steps included in the observation operator have a very relevant role in the verification of 2-metre temperature and relative humidity: One step is the averaging of subgrid surface variables over land fractions. The other one is the vertical interpolation of atmospheric profiles from model orography to the station height.

Figure 1 shows the big impact of the procedure followed to compute the postprocessed model 2-metre temperature on the observation verification scores. One procedure consists of comparing the observed 2-metre temperature value against the corresponding model output from the most predominant land fraction in the grid square. The other one compares the observed value against the areal average of 2-metre temperature over all existing fractions. The scores shown in Figure 1 correspond to 6 hours forecasts over the highly heterogeneous Scandinavian area (mainly due to the presence of lakes). The second alternative very much influenced by water tiles gives clearly worse scores both for bias and rms error, due to the fact that the stations are mainly representative of the land tiles. Besides, lake water temperature is only initialized using climatic values due to the lack of observations. Other posible alternatives, as the use of areal average only over land fractions or the use of the low vegetation fraction (closer to WMO specifications for SYNOP measurements), have been been tried (not shown here) and they do not show such big impact as the inclusion of the water fraction. The current version of the code computes for the diagnosed screen variables two types of areal average: i) over all existing fractions (water and ice included) within the grid square and ii) only over land fractions. The first one, usually smoother, includes the damping effect of the

water tiles, whereas the second one is more appropriate for verification purposes as the SYNOP stations used for verification are located over land.

The impact of vertical interpolation of the atmospheric profiles on the verification scores is crucial over certain mountainous areas. In fact, the lack of vertical interpolation usually produces some slight cold bias due to the higher model orography than the real station height. This difference can be explained by the fact that over mountainous regions observing stations are usually located at the bottom of valleys, frequently represented with higher altitude by models.

The observation statistics files generated by the surface analysis package are normally used to check the assimilation system performance and to monitor observations. It can be additionally used to test different verification strategies. One strategy would be to compare observations of 2-metre temperature and relative humidity against the output from the observation operator. Another alternative strategy, closer to the current verification package, could be to compare observations against the ouput from the observation operator but without any vertical interpolation from the model height to the real observation height. Figures 2 and 3 compare both verification strategies for H+6 forecasts of 2-metre temperature and relative humidity, respectively. The effect of the height correction is very noticeable for 2-metre temperature over mountainous areas. E.g., over the Spanish verification area, bias is corrected up to $1K$ and rms error is reduced up to $0.8K$. The Scandinavian and France areas also show the big impact of height correction in the verification scores.

Figure 4 shows the difference between the station height and the corresponding model height versus difference of 2-metre temperature bias for the two verification strategies (with and without vertical correction) mentioned above. Different verification times (00 and 12 UTC) and different areas are shown separately. Also the standard lapse rate correction of $0.65K/100m$ is shown to be a reasonable approximation. As it can be seen from Fig. 4, the procedure used in the 2-metre temperature observation operator allows for a time of the day and a day to day variation of the temperature vertical correction.

The complexity introduced in the model by the tiling structure allows many different alternatives for the verification algorithms, which have still to be explored and exploited. The few examples described here show that there is still a lot of room for the improvement of the verification procedures, in particular over highly heterogeneous terrain.

8 Parallel runs: verification and validation

The new surface scheme together with the related surface analysis and soil assimilation package has been debugged, tuned and tested during the last couple of years. A set of parallel test runs with a system employing a developed new scheme and an existing reference system is an efficient method of debugging and tuning.

Parallel tests with the old HIRLAM reference surface scheme and the new scheme have been carried out at INM and FMI. The INM tests have been carried out for the HIRLAM Delayed Mode Run (DMR) domain covering most of Europe. The FMI tests have been run for a Nordic area. Figure 5 shows both domains. The early tests, several years ago, were conducted with the

HIRLAM 2.7 and 4.1 systems and later on 4.6.2 and 5.0.0 systems were used. These runs helped to detect several problems and deficiencies and thus improved the new scheme. Furthermore, these test runs helped to find a few code portability problems as well as to speed up the code on different computer platforms. Some results from those tests have been reported in, e.g., Järvenoja (1998, 1999, 2002a, 2002b), Rodriguez *et al.* (2001), Rodriguez *et al.* (2002), Navascues *et al.* (2001). The new tiled surface scheme together with the related surface analysis and soil assimilation package has now been accepted into the HIRLAM Reference system as version 5.2. In the following, the latest results from parallel tests for the DMR domain and for the Nordic test domain using the old reference surface scheme and the new tiled scheme will be summarized.

8.1 DMR domain parallel experiments

The results presented here are based on the HIRLAM version 5.1.1 for the 'reference' and the new tiled scheme. The two parallel experiments, differing only in the surface treatment, are as follows:

- DMR : old reference surface scheme (HIRLAM 5.1.1)
- DMI : new tiled surface scheme together with the new surface analysis and soil assimilation.

The common features for the two experiments are:

- Domain: Area corresponding to the DMR HIRLAM suite with a 0.5° horizontal resolution
- 166 * 130 grid points; 31 levels in the vertical
- Semi-Lagrangian advection, dt = 10 min
- Each suite with its own data assimilation (OI, 6 h cycling)
- Lateral boundary conditions: ECMWF analyses
- 48 h forecasts from 00 UTC analyses only
- Periods: 1-15 January 1996, 15-30 April 1995, 1-15 July 1995 and 1-15 October 1994.

The INM parallel tests were conducted for two weeks periods in each of the four seasons. The January 1996 period represents a cold Nordic winter with snow covering Northern and Central Europe for most of the period. This period has been simulated in both implementations, but using different domains and horizontal resolutions. The April 1995 case was selected to study the quick irruption of warming and snow melting in Nordic latitudes. July 1995 represents the typical summer conditions in Southern Europe, with mainly warm and dry weather. Finally, October 1994 brings precipitation and allows to recharge the reservoir of soil water content in Central and Northern Europe, whereas the Iberian Peninsula still maintains dry summer conditions.

In the following, some results from the parallel experiments are presented for each test period: winter, spring, summer and autumn. Results are mainly focused on near-surface parameters, in particular 2-metre temperature (T_{2m}) and 2-metre relative humidity (RH_{2m}).

i) Winter: January 1996

The observation verification scores, bias and rms error as computed against EWGLAM stations for the January 1996 period are shown in Fig. 6 for T_{2m} (top left) and RH_{2m} (top right), respectively. As the long forecasts were run from the 00 UTC analyses, the forecast lengths of 24 and 48 h are verifying at night-time (00 UTC) and forecast lengths of 12 and 36 h at daytime (12 UTC). The experiment DMR shows a T_{2m} positive bias, whereas the bias is slightly negative in case of the DMI experiment. The rms error is smaller in DMI for all forecast lenths. The new surface scheme experiment (DMI) shows a RH_{2m} bias close to zero as opposed to the negative bias of the reference experiment (DMR), which is consistent with the clear reduction of rms error also in favour of the DMI experiment. Most of the improvement in the scores computed only over snow covered areas (not shown here) comes from the positive impact of soil temperature assimilation also allowed over snowed areas. As a whole, over the set of EWGLAM stations, the new surface (DMI) controls reasonable well bias of both T_{2m} and RH_{2m} and shows a clear reduction of rms errors of both variables.

ii) Spring: April 1995

This spring case shows again a remarkable tendency to keep biases of T_{2m} and RH_{2m} close to zero, as shown in Fig. 6 (2^{nd} row left and right, respectively). The rms error is slightly reduced in the new surface (DMI) with respect to the old reference surface (DMR), mainly at noon (forecast lengths of 12 and 36 h). These results are consistent with and similar to the other spring case (April 1998) run with the Nordic implementation and described below in more detail.

iii) Summer: July 1995

Figure 7 shows bias and rms error of 6 h forecasts for a 3-month period starting on 1^{st} July 1995. The scores are again referred to the set of EWGLAM observations. In summer time the evolution of soil water content is crucial to estimate the partition of surface heat fluxes and therefore of T_{2m} and RH_{2m}. As soil water content in the old surface package is mainly forced by model precipitation and radiation (the old surface scheme has no assimilation of soil water!), apart from other possible problems in the scheme, any bias or inaccuracy in the parameterization of condensation or radiation processes will be inherited by the evolution of soil water and it will be manifested as a drift of T_{2m} and RH_{2m}. Figure 7 for the month of September (bottom figures) shows some noticeable bias of T_{2m} and RH_{2m} towards warmer and drier values in the old reference surface (DMR), which is nicely controlled by the new scheme (DMI). Scores of bias and rms error for the first two weeks of the summer 1995 period (see 3^{rd} row left and right of Figure 6) show the same features described for the spring period, but more highlighted. As a summary of the summer period, it can be said that T_{2m} and RH_{2m} are mainly unbiased for the new surface treatment (DMI). One of the main features of the new surface package is the sequential assimilation of soil water content. As it was mentioned in the corresponding section, the assimilation of soil water content is only applied when synoptic conditions are such that 6 h forecast errors of screen variables are informative of the partition of radiative fluxes absorbed by land-surface between latent and sensible heat. Such partition is mainly controlled by soil water content. These synoptic conditions are mainly summerlike conditions, *i.e.*, dry weather, no strong advection, no cloudiness, etc. With such constraints in the assimilation of soil water one would expect more benefit in summer time and in Southern latitudes.

iv) Autumn: October 1994

The October 1995 case further confirms the good control of biases in a rainy period over most of Central and Northern Europe. It must be mentioned here that inaccuracies in the precipitation forecasts and its effect on soil moisture evolution can be compensated by the soil moisture assimilation algorithm (Douville *et al.*, 2000).

8.2 Nordic domain parallel experiments

The results presented below are based on the latest parallel runs that have been carried out using the HIRLAM version (5.1.2) and the β version (5.1.4) for 'reference' and 'new surface' runs, respectively. Again, the two parallel experiments, differing only in the surface treatment, are as follows:

- REL : old reference surface scheme (HIRLAM 5.1.2)
- ISL : new tiled surface scheme together with the new surface analysis and soil assimilation (HIRLAM 5.1.4)

The common features for the two experiments are:

- Domain: Area corresponding to the FMI operational European suite (ENO) with a 0.2° horizontal resolution
- 198 * 140 grid points; 31 levels in the vertical
- Semi-Lagrangian advection, dt = 5 min
- Each suite with its own data assimilation (OI, 6 h cycling)
- Lateral boundary conditions: ECMWF analyses
- 48 h forecasts from 12 UTC analyses only
- Periods: 1-15 January 1996, 12-26 April 1998 and 6-17 June 1997

The FMI parallel tests have been carried out for three different seasons. January 1996 represents a cold Nordic winter case with a high pressure dominating over Russia and northern Europe, and a low pressure area over the Atlantic. The April 1998 case is an example of a rapid warming and snow melt in northern Europe. This case highlights severe problems of the present reference system in spring at high latitudes: a substantial negative bias in predicted surface and 2-metre temperature. Finally, June 1997 represents a warm summer situation with convective activity.

In the following, some results from the parallel experiments are presented for each test period: winter, spring and summer. The focus in the results is the near-surface parameters, the 2-metre temperature (T_{2m}) and the 2-metre relative humidity (RH_{2m}) in particular. Observation verification as well as field verification scores will be presented, and examples from systematic differences between parallel runs will be shown.

i) Winter: January 1996

The observation verification scores, bias and standard deviation as computed against EWGLAM stations for the January 1996 period are shown in Fig. 8 for T_{2m} (top left) and RH_{2m} (top right), respectively. As the long forecasts were run from the 12 UTC analyses, the forecast lengths of 24 and 48 h are verifying at daytime (12 UTC) and forecast lengths of 12 and 36 h at night-time (00 UTC). Both experiments, REL and ISL show a T_{2m} negative bias, but the bias is smaller in case of the ISL experiment. The standard deviation is also smaller in ISL, especially at shorter forecast lengths. Both experiments show a small positive RH_{2m} bias, with ISL being less biased. On the other hand, the REL experiment shows s smaller standard deviation compared to ISL. As a whole, the ISL experiment is slightly better than REL in terms of these two near-surface variables.

ii) Spring: April 1998

The T_{2m} bias (Fig. 8, middle left) for REL varies between -0.5 and -1$^{\circ}C$, being more negative during daytime. However, if the verification is done against Scandinavian stations only, the bias is close to -3$^{\circ}C$ at daytime! The bias of the ISL experiment is centered around zero, but has a diurnal cycle being positive during daytime and negative during night-time. The standard deviation is smaller in case of ISL compared to REL. The RH_{2m} bias (Fig. 8, middle right) is positive for both runs, but the REL bias is clearly larger, more than 10% during daytime. In terms of the standard deviation, the REL experiment seems to better than ISL. As a whole, due to the smaller biases, the ISL experiment is superior to REL.

As the observation verification revealed, the predicted T_{2m} forecasts from the REL system showed a clear negative bias while the ISL system had practically no bias. The observation verification, when compressed to a single number as is shown in, *e.g.*, Fig. 8 (middle left), does not tell anything about the geographical distribution of the bias. The 2-metre temperature is now analyzed in the ISL experiment with the aid new surface analysis scheme, and as the analysis draws close to the observed T_{2m}, this analyzed field can be used as the verifying field for the T_{2m} forecasts, for both experiments REL and ISL. Figure 9 shows the geographical distribution of the T_{2m} bias for the REL experiment for the two-week period in April 1998. The general outlook is terrible. For most of the land area the bias is negative and it is really large, being as much as -7$^{\circ}C$ at worst, over areas of Finland, Sweden, Estonia and western parts of Russia. In single cases, the forecast error can be as much as -15$^{\circ}C$, which is unacceptable. Figure 10 shows the corresponding bias field for the ISL experiment. The difference to Fig. 9 is drastic: the large negative bias seen in the REL experiment has almost disappeared. There remains a bias of -1...-2$^{\circ}C$ in northern Europe, while the positive bias in southern latitudes is slightly larger. As a whole, the ISL experiment shows a tremendous improvement compared to REL.

The cold bias in the REL experiment is not limited only to the surface, but extends further up to 925 hPa. The field verification reveals that there is a bias of -1...-3$^{\circ}C$ over southern Finland, Estonia and western Russia (not shown). However, there is practically no temperature bias at 850 hPa.

The different behavior of the REL and ISL runs can be highlighted with the aid of model profiles (soundings) from 24 h forecasts of respective experiments for a grid point close to the Luonetjärvi station (62° 24'N, 25° 41'E) in central Finland for 12 UTC 26 April 1998, as shown in Fig. 11. In the REL profile, there is an inversion at 925 hPa and below 950 hPa saturation occurs. The low-level cloud deck prevents the SW radiation from reaching the ground and thus results in low near-surface temperatures. The predicted surface temperature (or T_{2m}) is only 4$^{\circ}C$, which is about 10$^{\circ}C$ colder than observed. The main reason for the cold bias in the REL experiment is

the excessive evaporation, which in turn leads to formation of low clouds. The ISL profile is very different. There is no sign of an inversion, the temperature and the dewpoint temperature are well separated from each other and the temperature profile below 900 hPa follows the dry-adiabatic. The predicted surface temperature is $15^{\circ}C$, which is in a good agreement with the observation. Evaporation in the ISL experiment is smaller than in REL leading to lower near-surface humidity and less clouds.

iii) Summer: June 1997

Figure 8 (bottom) shows the observation verification scores for the June 1997 period. Both experiments show a slight positive bias on average, but there is a clear diurnal cycle as well. There is a positive T_{2m} bias of $0.5^{\circ}C$ in the REL experiment (Fig. 8 (bottom left) at night-time (12 and 36 h), while the ISL experiment shows a similar bias in the morning (18 and 42 h). The ISL run shows a slight negative bias at night-time (12 and 36 h). The ISL run is somewhat better in terms of the standard deviation. Figure 8 (bottom right) shows that there is a negative RH_{2m} bias in the REL experiment at all verifying times, while there is diurnal cycle (centered around zero) in the ISL run, at the opposite phase to the T_{2m} bias. In terms of the standard deviation, the ISL run is again superior. Examples of systematic differences between ISL and REL forecasts are given in Figures 12 and 13, which demonstrate differences of accumulated precipitation and cloud cover in 48 h forecasts (ISL-REL), respectively. The ISL experiment gives about 2 mm more precipitation in 48 hours (corresponding to 30 mm in a month) over Russia north of the Black Sea than REL (Fig. 12), on average. This feature coincides with a larger (1 to 2 octas) daytime cloud cover in ISL as shown in Fig. 13. The lesser cloud cover in REL results in a higher daytime T_{2m} compared to ISL, and there is a positive bias of 1 - $3^{\circ}C$ in the REL experiment over continental areas, especially over Russia (not shown). There is generally only a small bias in the ISL experiment, except over mountainous areas where ISL has a positive bias of a few degrees locally (not shown).

9 Summary

The new package for the analysis of surface variables and parameterization of surface processes has been presented. The surface analysis provides initial values of the following variables: water surface temperature, fraction of water and ice, snow depth, 2-metre temperature, 2-metre relative humidity, surface soil temperature, mean soil temperature, surface soil water content and total soil water content. Both the analysis and the parameterization part treat the high surface heterogeneity by making use of a tiled structure within each grid square. The current version of the code allows up to five different tiles (water, sea ice, bare ground, low vegetation, forest), although the upgrading to a bigger number of tiles is straighforward. The ISBA scheme was selected to model land surface tiles.

Parallel tests with the old HIRLAM reference surface scheme and with the new tiled surface scheme have been carried out for three different seasons in a Nordic area with 20 km horizontal resolution and for four different seasons in the Delayed Mode Run (DMR) area with 50 km horizontal resolution. The resulting forecasts have been validated by means of observation and field verification. The winter period (1-15 January 1996), which was run using both domains, shows some slight differences in connexion with 2-metre temperature biases. These differences are easily explained considering that most of Southern Europe stations are not included in the Nordic implementation.

The main focus in the forecast validation has been the near-surface parameters, the 2-metre temperature in particular, due to their importance for duty forecasters. The verification results have shown that the new tiled scheme results in better T_{2m} forecasts compared to the old reference surface scheme, especially in spring time for the Nordic simulations and in summer time for the DMR simulations. Also some positive impact can be seen in the rest of the periods simulated. The long-lasting problem of dramatic 2-metre temperature biases, in particular the cold bias in springtime, has been solved to a great extent with the introduction of the new tiled surface scheme. The scores for upper-air parameters were very similar for new and old surface treatments and for all test periods.

Acknowledgments. The authors are very grateful to Björn Bringfelt, who first started a preliminary version of the HIRLAM tiled surface scheme and proposed many of the ideas still present in the current code, to Bart van den Hurk, who re-coded a substantial part of parameterization part, to Dominique Giard, Eric Bazile and Gianpaolo Balsamo, for the very useful exchange of ideas and the stimulating years of joint work, to Stefan Gollvik, who has shed light on the problems related with the snow formulation, to Anne Jochum, who has scrutinized the manuscript and suggested improvements to the text and to many other HIRLAM colleagues (too many to be named here) for the illuminating discussions which have helped us to improve the formulation of the code. Finally, we also thank to Per Unden and one anonymous reviewer for their constructive comments on the original manuscript.

10 References

1. André, J.C. and Blondin, C. 1986. On the effective roughness length for use in numerical three-dimensional models. *Bound.-Layer Met.*, **35**, 231-245.

2. André, J.C., Bougeault, P., Mahfouf, J.F., Mascart, P., Noilhan, J. and Pinty, J.P. 1989. Impact of forest on mesoscale meteorology. *Phil. Trans. R. Soc. Lond. B*, **324**, 407-422.

3. Armstrong, R. and Hardman, M. 1991. Monitoring global snow cover. *Proc. 1991 International Geoscience and Remote Sensing Symposium*, Espoo, Finland, IEEE, 1947-1950.

4. Avissar, R. and Pielke, R.A. 1989. A parameterization of heterogeneous land surfaces for atmospheric numerical models and its impact on regional meteorology. *Mon. Wea. Rev.*, **117**, 2113-2136.

5. Avissar, R. 1992. Conceptual aspects of a statistical-dynamical approach to represent landscape subgrid-scale heterogeneities in atmospheric models. *J. Geophys. Res.*, **97**, 2729-2742.

6. Avissar, R. and Liu, Y. 1996. A three-dimensional study of shallow convective clouds and precipitation induced by land-surface forcing. *J. Geophys. Res.*, **101**, 7499-7518.

7. Avissar, R. and Schmidt, T. 1998. An evaluation of the scale at which ground-surface heat flux patchiness affects the convective boundary layer using a Large-Eddy Simulation model. *J. Atmos. Sci.*, **55** 2666-2689.

8. Ayuso, J.J. 1995. Implementation of ASSISBA in the HIRLAM system. *Proceedings of the HIRLAM3 Workshop on soil processes and soil/surface data assimilation, 27-29 November 1995.* (Available from SMHI, S-60176 Norrköping, Sweden).

9. Balsamo, G., Bouyssel, F. and Noilhan, J. 2001. Mesoscale variational assimilation for land surface variables. *Proceedings of the SRNWP/HIRLAM Workshop on Surface Processes, Turbulence and Mountain Effects. Instituto Nacional de Meteorologia, Madrid, 22-24 October 2001.* (Available from SMHI, S-60176 Norrköping, Sweden).

10. Betts, A.K., Viterbo, P., Beljaars, A.C.M. and van den Hurk, B.J.J.M. 2001. Impact of BOREAS on the ECMWF Forecast Model. *J. Geophys. Res.*, **106**, 33,593-33,604.

11. Blyth, E.M., Dolman, A.J. and Wood, N. 1993. Effective resistance to sensible and latent heat flux in heterogeneous terrain. *Q.J.R. Meteorol. Soc.*, **119**, 423-442.

12. Blondin, C. 1991. Parameterization of land-surface processes in numerical weather prediction. *Land surface evaporation: measurement and parameterization*, T.J. Schmugge and J.C. André, Eds., Springer, 31-54.

13. Bougeault, P., Bret, B., Lacarrere, P., Noilhan, J. 1991. An experiment with an advanced surface parameterization in a meso-beta-model. Part II: the 16 June 1986 simulation. *Mon. Wea. Rev.*, **119**, (10), 2374-2392.

14. Bouttier F., Mahfouf, J.-F. and Noilhan, J. 1993a. Sequential Assimilation of Soil Moisture from Atmospheric Low-Level Parameters. Part I: Sensitivity and Calibration Studies. *J. Appl. Meteor.*, **32**, 1335-1351.

15. Bouttier F., Mahfouf, J.-F. and Noilhan, J. 1993b. Sequential Assimilation of Soil Moisture from Atmospheric Low-Level Parameters. Part II: Implementation in a Mesoscale Model. *J. Appl. Meteor.*, **32**, 1352-1364.

16. Brasnett, B. 1999. A global analysis of snow depth for numerical weather prediction. *J. Appl. Meteor.*, **38**, 726-740.

17. Braud, I., Noilhan, J., Bessemoulin, P., Mascart, P., Haverkamp, R. and Vauclin, M. 1993. Bare-ground surface heat and water exchanges under dry conditions: observations and parameterization. *Boundary-Layer Meteorol.*, **66**, 173-200.

18. Bringfelt, B. 1996. Test of a new land-surface treatment in HIRLAM. *HIRLAM Technical Report No 23*, Norrköping, Sweden. [Available from B. Bringfelt, SMHI, S-60119 Norrköping, Sweden].

19. Bringfelt B., Heikinheimo M., Gustafsson N., Perov V. and Lindroth A. 1999. A new land surface treatment for HIRLAM - Comparisons with NOPEX measurements. *Agricultural and Forest Meteorology.*

20. Carson, D.J., and Sangster, A.B. 1981. The influence of land-surface albedo and soil moisture on general circulation model simulations. GARP/WCRP: Research Activities in Atmospheric and Oceanic Modeling. I.D. Rutherford, Eds., Numerical Experimentation Programme, Report No. 2, 5.14-5.21.

21. Champeaux, J.-L., Arcos, D., Bazile, E., Giard, D., Goutorbe, J.-P., Habets, F., Noilhan, J. and Roujean, J.-L. 2000. AVHRR-derived vegetation mapping over Western Europe for use in Numerical Weather Prediction models. *Int. J. Remote Sensing.*, **21**, 1183-1199.

22. Charney, J.G., Quirk, W.J., Chow, S.H. and Kornfield, J. 1977. A comparative study of the effects of albedo on drought in semi-arid regions. *J. Atmos. Sci.*, **34**, 1366-1385.

23. Charnock, H. 1955. Wind stress on a water surface. *Q.J.R. Meteorol. Soc.*, **81**, 639-640.

24. Chen, F. and Avissar, R. 1994a. Impact of land-surface moisture variability on local shallow convective cumulus and precipitation in large-scale models. *J. Appl. Meteor.*, **33**, 1382-1401.

25. Chen, F. and Avissar, R. 1994b. The impact of land-surface wetness heterogeneity on mesoscale heat fluxes. *J. Appl. Meteor.*, **33**, 1323-1340.

26. Chen, F. and Coauthors. 1996. Modelling of land-surface evaporation by four schemes and comparison with FIFE observations. *J. Geophys. Res.*, **101**, 7251-7268.

27. Chen, F. and Coauthors. 1997. Cabauw experimental results from the Project for Intercomparison of Land-surface Parameterization Schemes. *J. Climate*, **10**, 1194-1215.

28. Chervin, R.M. 1978. Response of the NCAR general circulation model to change land-surface albedo. Report of the JOC Study Conference on Climate Models: Performance, Intercomparison and Sensitivity Studies, Washington, DC, GARP Publ. Series, No 22, Vol 1, 563-581.

29. Clapp, R.B. and Hornberger, G.M. 1978. Empirical equations for some soil hydraulic properties. *Water Resour. Res.*, **14**, 601-604.

30. Claussen, M. 1990. Area-averaging of surface fluxes in a neutrally stratified, horizontally inhomogeneous atmospheric boundary layer. *Atmos. Environ.*, **24a**, 1349-1360.

31. Claussen, M. 1991. Estimation of areally-averaged surface fluxes. *Bound.-Layer Met.*, **54**, 387-410.

32. Claussen, M. 1995. Flux aggregation at large scales. On the limits of validity of the concept of blending height. *J. Hydrology*, **166**, 371-382.

33. Coiffier, J., Ernie, Y., Geleyn, J.-F., Clochard, J., Hoffman, J., and Dupont, F. 1987. The operational hemispheric model at the French meteorological service. *J. Met. Soc. Japan, Special Issue on Short and Medium Range Numerical Weather Prediction*, 337-345.

34. Côté, J., Gravel, S. , Méthot, A., Tatoine, A., Roch, M., Staniforth, A. 1998. The operational CMC-MRM Global Environmental Multiscale (GEM) model. Part I: Design considerations and formulation. *Mon. Wea. Rev.*, **126**, 1373-1395.

35. Cox, P.M., Betts, R.A., Bunton, C.B., Essery, R.H.S., Rowntree, P.R. and Lean, J. 1999. The impact of the new land surface physics on the GCM simulation of climate and climate sensitivity. *Climate Dynamics*, **15**, 183-203.

36. Daley, R. 1991. *Atmospheric data analysis.* Cambridge Univ. Press, Cambridge, 458 pp.

37. Deardorff, J.W. 1978. Efficient prediction of ground surface temperature and moisture, with inclusion of layer a of vegetation. *J. Geophys. Res.*, **83C**, 1889-1903.

38. Decoudré, N.I., Laval, K. and Perrier, A. 1993. SECHIBA, a new set of parameterizations of the hydrologic exchanges at the land-atmosphere interface within the LMD atmospheric general circulation model. *J. Climate*, **6**, 248-273.

39. Dickinson, R.E. 1988. The force-restore model for surface temperatures and its generalizations. *J. Climate*, **1**, 1086-1097.

40. Dickinson, R.E. and Henderson-Sellers, A. 1988. Modelling tropical deforestation, a study of GCM land-surface parameterizations. *Quart. J. R. Met. Soc.*, **114**, 439-462.

41. Dickinson, R.E. 1993. Biosphere-Atmosphere Transfer Scheme (BATS) Version 1e as coupled to the NCAR community climate model, *NCAR Technical Note/ NCAR TN-387+STR*, National Center for Atmospheric Research, Boulder, Colorado. [Available from R. E. Dickinson, Department of Atmospheric Physics, University of Arizona, Tucson, AZ.]

42. Dolman, A.J. 1993. A multiple source energy balance model for use in general circulation models of the atmosphere. *Agric. For. Meteorol.*, **65**, 21-45

43. Dolman, A.J. and Blyth, E.M. 1997. Patch scale aggregation of heterogeneous land surface cover for mesoscale meteorological models. *J. Hydrology*, **190**, 252-268.

44. Douville, H., Royer, J.F. and Mahfouf, J.F. 1995. A new snow parameterization for the Météo-France climate model. Part I: validation in stand-alone experiments. *Clim. Dyn.*, **12**, 21-35.

45. Douville, H., Viterbo, P., Mahfouf, J.-F. 2000. Evaluation of the Optimum Interpolation and Nudging Techniques for the Soil Moisture Analysis Using FIFE Data. *Mon. Wea. Rev.*, **128**, 1733-1756.

46. Ducharne, A., Koster, R.D., Suarez, M.J., Stieglitz, M. and Kumar, P. 2000. A catchment-based approach to modelling land surface processes in a general circulation model. Part II: Parameter estimation and model demonstration. *J. Geophys. Res.*, **105**, 24823-24838.

47. Eerola, K. 1995. Experiences with the analysis of sea surface temperature, ice coverage and snow depth. *Proceedings of the HIRLAM3 Workshop on soil processes and soil/surface data assimilation, 27-29 November 1995.* (Available from SMHI, S-60176 Norrköping, Sweden).

48. Entekhabi, D. and Eagleson, P.S. 1989. Land surface hydrology parameterization for atmospheric general circulation models including subgrid scale spatial variability. *J. Climate*, **2**, 816-831.

49. Famiglietti, J.S. and Wood, E.F. 1994. Multi-scale modeling of spatially- variable water and energy balance processes. *Water Resour. Res.*, **30**, 3061-3078.

50. Garratt, J.R. 1992. *The atmospheric boundary layer.* Cambridge Atmospheric and Space Science Series. Cambridge University Press, Cambridge, U.K., 316 pp.

51. Garratt, J.R. 1993. Sensitivity of climate simulations to land-surface and atmospheric boundary layer treatments - A review. *J. Climate*, **6**, 419-449.

52. Geleyn, J.-F. 1988. Interpolation of wind, temperature and humidity values from model levels to the height of measurement. *Tellus*, **40A**, 347-351.

53. Giard, D. and Bazile, E. 2000. Implementation of a new assimilation scheme for soil and surface variables in a global NWP model. *Mon. Wea. Rev.*, **128**, 997-1015.

54. Giordani, H. 1993. Expériences de validacion unidimensionnelles du schéma de surface NP89 aux normes ARPEGE sur trois sites de la campagne EFEDA 91. *Note de Centre No. 24.* CNRM (Météo-France), (Available from Météo-France, 31057 Toulouse, France).

55. Giorgi, F. 1997a. An approach for the representation of surface heterogeneity in land surface models. Part I: Theoretical framework. *Mon. Wea. Rev.*, **125**, 1885-1899.

56. Giorgi, F. 1997b. An approach for the representation of surface heterogeneity in land surface models. Part II: Validation and sensitivity experiments. *Mon. Wea. Rev.*, **125**, 1900-1919.

57. Gustafsson, N. 1985. Development of mesoscale analysis scheme for nowcasting and very short range forecasting. *Proceedings of the ECMWF Workshop on High Resolution Analysis, Reading, 24-26 June 1985, 183-212.* (Available from ECMWF, Shinfield Park, Reading, Berkshire RG2 9AX, UK.).

58. Hallikainen, M. 1996a. Physical basis for microwave remote sensing of sea ice and snow. *Radiation and water in the climate system*, T.J.E. Raschke, Ed., Springer, 527-549.

59. Hallikainen, M. 1996b. Retrieval of sea ice and snow parameters from microwave radiometer and radar data.*Radiation and water in the climate system*, T.J.E. Raschke, Ed., Springer, 527-549.

60. Henderson-Sellers, A. 1993. A factorial assessment of the sensitivity of the BATS land-surface parameterization scheme. *J. Climate*, **6**, 227-247.

61. Henderson-Sellers, A. 1996a. Soil moisture: a critical focus for global change studies. *Global and Planetary Change*, **13**, 3-9.

62. Henderson-Sellers, A. 1996b. Soil moisture simulation: achievements of the RICE and PILPS intercomparison workshop and future direccions. *Global and Planetary Change*, **13**, 99-115.

63. Henderson-Sellers, A. 1996c. Soil moisture: the land-surface "connexion" in GOALS, in GOAL Symposium, pp. 107-110, American Meteorological Society.

64. Hess, R. 2000. Variational Soil Moisture Analysis with First Operational Results. *Quarterly Report of the Operational NWP-Models of the Deutcher Wetterdienst*, **22**, 8-15.

65. van den Hurk, B.J.J.M, Viterbo, P., Beljaars, A.C.M. and Betts, A.K. 2000. Offline validation of the ERA40 surface scheme. *Technical Memorandum No.***295**, ECMWF. (Available from ECMWF, Shinfield Park, Reading, Berkshire RG2 9AX, UK.).

66. Järvenoja, S., 1998. Parallel test runs HIRLAM 4.1 vs. 2.7 at FMI. *HIRLAM Newsletter*, **30**, 20-28.

67. Järvenoja, S., 1999. Testing of the ISBA surface scheme - a Nordic winter case. Proceedings of the HIRLAM 4 Workshop on Physical Parameterization, INM, Madrid 11-13 November 1998, 144-150.

68. Järvenoja, S., 2002a. ISBA tests in a Nordic area. Proceedings of the SRNWP/HIRLAM Workshop on Surface Processes, Turbulence and Mountain Effects, INM, Madrid 22-24 October 2001, 64-74.

69. Järvenoja, S., 2002b. ISBA tests in a Nordic area - an update. *HIRLAM Newsletter*, **41**, 63-73.

70. Jarvis, P.G. 1976. The interpretation of the variation in leaf water potential and stomatal conductance found in canopies in the field. *Phil. Trans. Roy. Soc. London*, **B273**, 593-610.

71. Kabat, P., Hutjes, R.W.A., Feddes, R.A. 1997. The scaling characteristics of soil parameters: From plot scale heterogeneity to subgrid parameterization. *J. Hydrology*, **190**, 363-396.

72. Källen, E. (ed.) 1996. HIRLAM Documentation Manual, System 2.5. SMHI. Norrköping. (Available from SMHI, S-60176 Norrköping, Sweden).

73. Koster, R.D. and Suarez, M.J. 1992. A comparative analysis of two land surface heterogeneity representations. *J. Climate*, **5**, 1379-1390.

74. Koster, R.D., Suarez, M.J., Ducharne, A., Stieglitz, M. and Kumar, P. 2000. A catchment-based approach to modelling land surface processes in a general circulation model. Part I: Model structure. *J. Geophys. Res.*, **105**, 24809-24822.

75. Li, B. and Avissar, R. 1994. The impact of spatial variability of land-surface characteristics on land-surface heat fluxes. *J. Climate*, **7**, 527-537.

76. Louis, J.-F., Tiedtke, M. and Geleyn, J.-F. 1982. A short story of the PBL parameterization at ECMWF. *Proceedings of the ECMWF Workshop on Planetary Boundary Layer Parameterization, 25-27 November 1981. Technical Report, ECMWF, 59-80.* (Available from ECMWF, Shinfield Park, Reading, Berkshire RG2 9AX, UK.).

77. Mahfouf, J.F., Richard, E. and Mascart, P. 1987. The influence of soil and vegetation on the development of mesoscale circulations. *J. Climate Appl. Meteor.*, **26**, 1483-1495.

78. Mahfouf, J.-F. 1991. Analysis of soil moisture from near-surface parameters: a feasibility study. *J. Appl. Meteorol.*,**30**, 1534-1547.

79. Mahfouf, J.-F. and Viterbo, P. 1996. Land surface assimilation. *Proceedings of the ECMWF Seminar on Data Assimilation. Reading, 2-6 September 1996.* (Available from ECMWF, Shinfield Park, Reading, Berkshire RG2 9AX, UK.).

80. Manabe, S. 1969. Climate and the ocean circulation, 1. The atmospheric circulation and the hydrology of the earth surface. *Mon. Wea. Rev.*, **97**, 739-774.

81. Mason, P.J., 1988. The formation of areally-averaged roughness lengths. *Q.J.R. Meteorol. Soc.*, **114**, 399-420.

82. Mintz, Y. 1984. The sensitivity of numerically simulated climates to land- surfaces conditions. In: *The Global Climate*, J. Houghton, Ed., Cambridge University Press, 79-105.

83. Miyakoda, K. and Strikler, R.F. 1981: Cumulative results of extended forecast experiments. Part III: Precipitation. *Mon. Wea. Rev.*, **109**, 830-842.

84. Navascues, B. 1997. Analysis of 2 m temperature and relative humidity. *HIRLAM Technical Report No 28*, Norrköping, Sweden. (Available from SMHI, S-60176 Norrköping, Sweden).

85. Navascues, B., Rodriguez, E. and Ayuso, J.J. 2002. The new HIRLAM surface analysis. Proceedings of the SRNWP/HIRLAM Workshop on Surface Processes, Turbulence and Mountain Effects, INM, Madrid 22-24 October 2001, 37-44.

86. Nielsen, N.W. 1999. A revised formulation of surface fluxes over sea. Proceedings of the HIRLAM 4 Workshop on Physical Parameterization, INM, Madrid 11-13 November 1998, 112-120.

87. Noilhan, J. and Planton, S. 1989. A simple parameterization of land surface processes for meteorological models. *Mon. Wea. Rev.*, **117**, 536-549.

88. Noilhan, J. and Lacarrere, P. 1995. GCM grid-scale evaporation from mesoscale modeling. *J. Climate*, **8**, 206-223.

89. Noilhan, J., Lacarrere,. P., Dolman, A.J., and Blyth, E.M. 1997. Defining area-average parameters in meteorological models for land surfaces with mesoscale heterogeneity. *J. Hydrol.*, **190**, 302-316.

90. Noilhan, J. and Mahfouf, J.F. 1996. The ISBA land surface parameterization scheme. *Global and Planetary Change*, **13**, 145-149.

91. Pielke, R.A., Lee, T.J., Copeland, J.H., Eastman, J.L., Ziegler, C.L. and Finley, C.A. 1997. Use of USGS-provided data to improve weather and climate simulations. *Ecol. Appl.*, **7**, 3-21.

92. Richardson, L.F. 1922. *Weather Prediction by Numerical Process.* Cambridge Univ. Press, reprinted Dover, 1965, 236 pp.

93. Rodriguez-Camino, E. and Avissar, R. 1998. Comparison of three land-surface schemes with the Fourier Amplitude Sensitivity Test (FAST). *Tellus*, **50A**, 313-332.

94. Rodriguez-Camino, E. and Avissar, R. 1999. Effective parameters to heat surface fluxes in heterogeneous terrain. *Tellus*, **51A**, 387-399.

95. Rodriguez, E., Järvenoja, S., Navascues, B. and Ayuso, J.J.. 2001. The ISBA scheme for HIRLAM5: latest results prior to the operational implementation. *HIRLAM Newsletter*, **38**, 61-69.

96. Rodriguez, E., Navascues, B. and Ayuso, J.J. 2002. The tiling surface scheme for HIRLAM5: features and latest results. Proceedings of the SRNWP/HIRLAM Workshop on Surface Processes, Turbulence and Mountain Effects, INM, Madrid 22-24 October 2001, 55-63.

97. Baidya Roy, S. and Avissar, R. 2000. Scales of response of the convective boundary layer to land-surface heterogeneity. *Geophys. Res. Lett.*, **27** 533-536.

98. Rowell, D.P. and Blondin, C. 1990. The influence of soil moisture distribution on short-range rainfall forecasting in the West African Sahel. *Quart. J. Roy. Meteor. Soc.*, **116**, 1471-1485.

99. Rowntree, P.R. and Bolton, J.A. 1993. Simulation of the atmospheric response to soil moisture anomalies over Europe. *Quart. J. Roy. Meteor. Soc.*, **1109**, 501-526.

100. Schmugge, T.J. and André, J.-C. (Eds.). 1991. *Land Surface Evaporation. Measurement and Parameterization.* Springer-Verlag, New York, U.S.A., 424 pp.

101. Schmugge, T.J. and Becker, F. 1991. Remote Sensing Observations for the Monitoring of Land-Surface Fluxes and Water Budgets. *Land Surface Evaporation. Measurement and Parameterization.* Schmugge, T.J. and André, J.-C. (Eds.). Springer-Verlag, New York, U.S.A., 337-347.

102. Sellers, P.J. 1985. Canopy reflectance, photosynthesis and transpiration. *Int. J. Remote Sensing*, **6**, 1335-1372.

103. Sellers, P.J., Mintz, Y., Sud, Y.C., Dalcher, A. 1986. A simple biosphere model (Sib) for use within general circulation models. *J. Atmos. Sci.*, **43**, 505-531.

104. Sellers, P.J., Heiser, M.D., Hall, F.G., Goetz, S.J., Strebel, D.E., Verma, S.V, Desjardins, R.L., Schuepp, P.M., MacPherson, I. 1995. Effects of spatial variability in topography, vegetation cover and soil moisture on area-averaged surface fluxes: a case study using FIFE 1989 data. *J. Geophys. Res.*, **100**, 25607-25629.

105. Sellers, P.J., Heiser, M.D., Hall, F.G., Verma, S.V, Desjardins, R.L., Schuepp, P.M., MacPherson, I. 1997. The impact of using area-averaged land surface properties- topography, vegetation condition, soil wetness- in calculations of intermediate scale (approximately 10 km^2) surface-atmosphere heat and moisture fluxes. *J. Hydrology*, **190**, 269-301.

106. Shao, Y. and Henderson-Sellers, A. 1996. Modelling soil moisture: A project for Intercomparison of Land Surface Parameterization Schemes.*J. Geophys. Res.*, **101**, 7227-7250.

107. Shukla, J. and Mintz, Y. 1982. Influence of Land-Surface Evapotranspiration on the Earth's Climate. *Science*, **215**, 1498-1501.

108. Sivapalan, M. and Woods, E.F. 1995. Evaluation of the effects of general circulation model's subgrid variability and patchiness of rainfall and soil moisture on land surface water balance fluxes. *Scale Issues in Hydrological Modeling*, J.D. Kalma and M. Sivapalan, Eds. John Wiley and Sons, 453-473.

109. Stössel, A. and Claussen, M. 1993. On the momentum forcing of a large-scale sea-ice model. *Climate Dyn.*, **9**, 71-80.

110. Sud, Y.C., Sellers, P.J., Mintz, Y., Chou, M.D., Walker, G.K. and Smith, W.E. 1990. Influence of the biosphere on the global circulation and hydrological cycle - A GCM simulation experiment, *Agric. For. Meteor.*, **52**, 1036-1054.

111. Shuttleworth, W.J. 1988. Macrohydrology - The new challenge for process hydrology. *J. Hydrology*, **100**, 31-56.

112. Taylor, P.A. 1987. Comments and further analysis on effective roughness lengths for use in numerical three-dimensional models. *Bound.-Layer Met.*, **39**, 403-418.

113. Viterbo, P. 1996. The representation of surface processes in general circulation models. Thesis submitted for the degree of Doutor em Fisica of the University of Lisbon. ECMWF. (Available from ECMWF, Shinfield Park, Reading, Berkshire RG2 9AX, UK.).

114. Viterbo, P., Beljaars, A., Mahfouf, J.F. and Teixeira, J., 1999. The representation of soil moisture freezing and its impact on the stable boundary layer. *Q. J. R. Meteorol. Soc.*, **125**, 2401-2426.

115. Walter, J. and Rowntree, P.R. 1977. The effect of soil moisture on circulation and rainfall in a tropical model. *Quart. J. Roy. Meteor. Soc.*, **103**, 29-46.

116. Wieringa, J. 1986. Roughness-dependent geographical interpolation of a surface wind speed averages. *Q.J.R. Meteorol. Soc.*, **112**, 867-889.

117. Wood, E.F., 1997. Effects of soil moisture aggregation on surface evaporative fluxes. *J. Hydrology*, **190**, 397-412.

118. Wood, N. and Mason, P.J. 1991. The influence of stability on effective roughness lengths for momentum and heat transfer. *Q.J.R. Meteorol. Soc.*, **117**, 1025-1056.

119. Wood, E.F. and Coauthors, 1998. The Project for Intercomparison of Land-surface Parameterization Schemes (PILPS). Phase 2(c) Red-Arkansas River Basin experiment: 1. Experiment description and summary intercomparisons. *Global Planetary Change*, **19**, 115-136.

120. Xue, Y., Sellers, P.J., Kinter, J.L. and Shukla, J. 1991. A simplified biosphere model for global climate studies. *J. Climate*, **4**, 346-364.

121. Xue, Y., Fenessy, M. and Sellers, P.J. 1996. Impact of vegetation properties on US weather prediction. *J. Geophys. Res.*, **101**, 7419-7430.

122. Xue, M., Wang, D.-H., Gao, J.-D., Brewster, K. and Droegemeier, K.K. 2001 The Advanced Regional Prediction System (ARPS), storm-scale numerical weather prediction and data assimilation. *Submitted to Meteor. Atmos. Physics.*

123. Yang, R., Fennessy, M.J. and Shukla, J. 1994. The influence of initial soil wetness on medium-range surface weather forecasts. *Mon. Wea. Rev.*, **122**, 471-485.

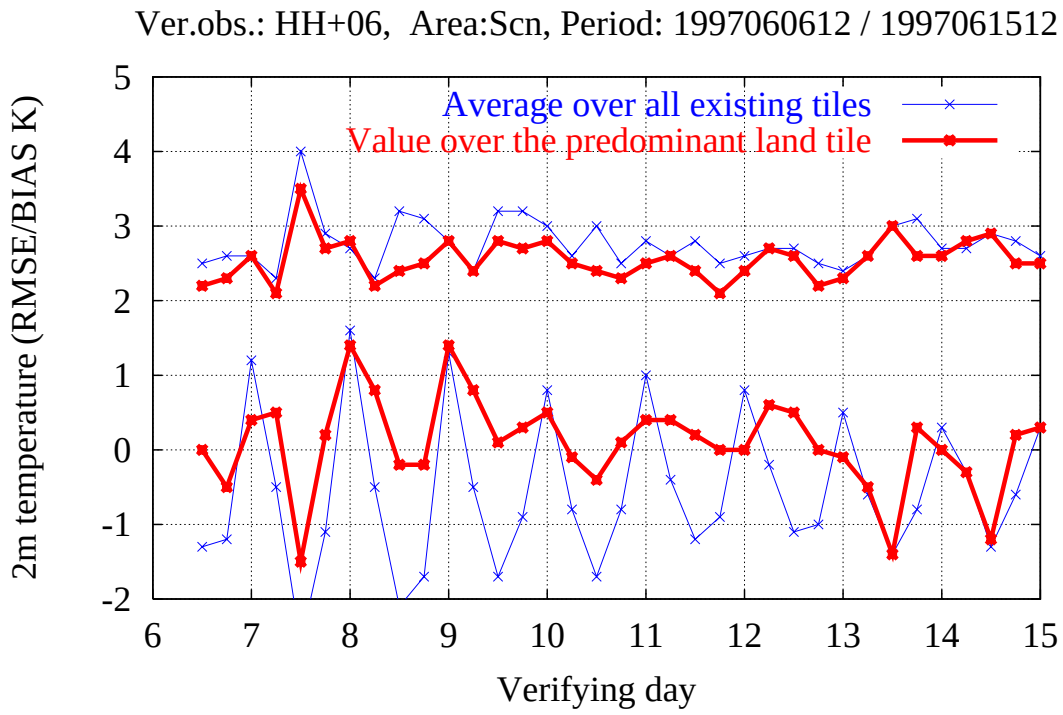

Figure 1: 2-metre temperature bias and rms error of H+6 forecasts using two different verification strategies: i) comparing observations against the most predominant land fraction and ii) comparing observations against the areal average over all existing fractions. Verification period: 6-15 June 1997. Verification area: Scandinavia

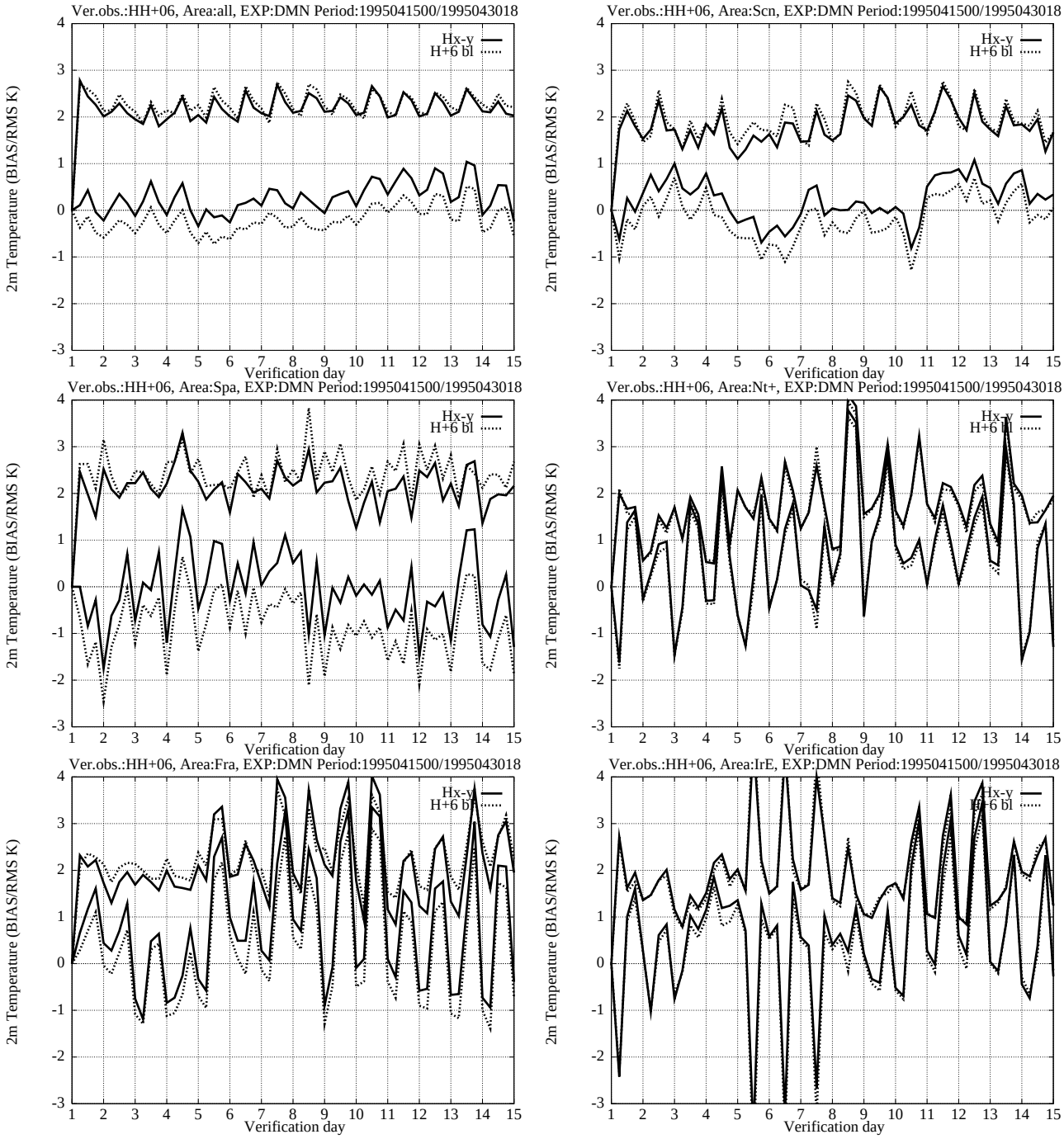

Figure 2: 2-metre temperature bias and rms error of H+6 forecasts using two different verification strategies: i) comparing observations directly against the horizontally interpolated model fields (dash lines) and ii) comparing observations against the horizontally interpolated model field and vertically corrected to the observation height (solid lines). Verification period: 15-30 April 1995. Different figures correspond to the verification areas in the HIRLAM reference system: all observations in the integration area, Scandinavia, Spain, Netherlands, France, Ireland. Only observations accepted by the analysis algorithm have been used.

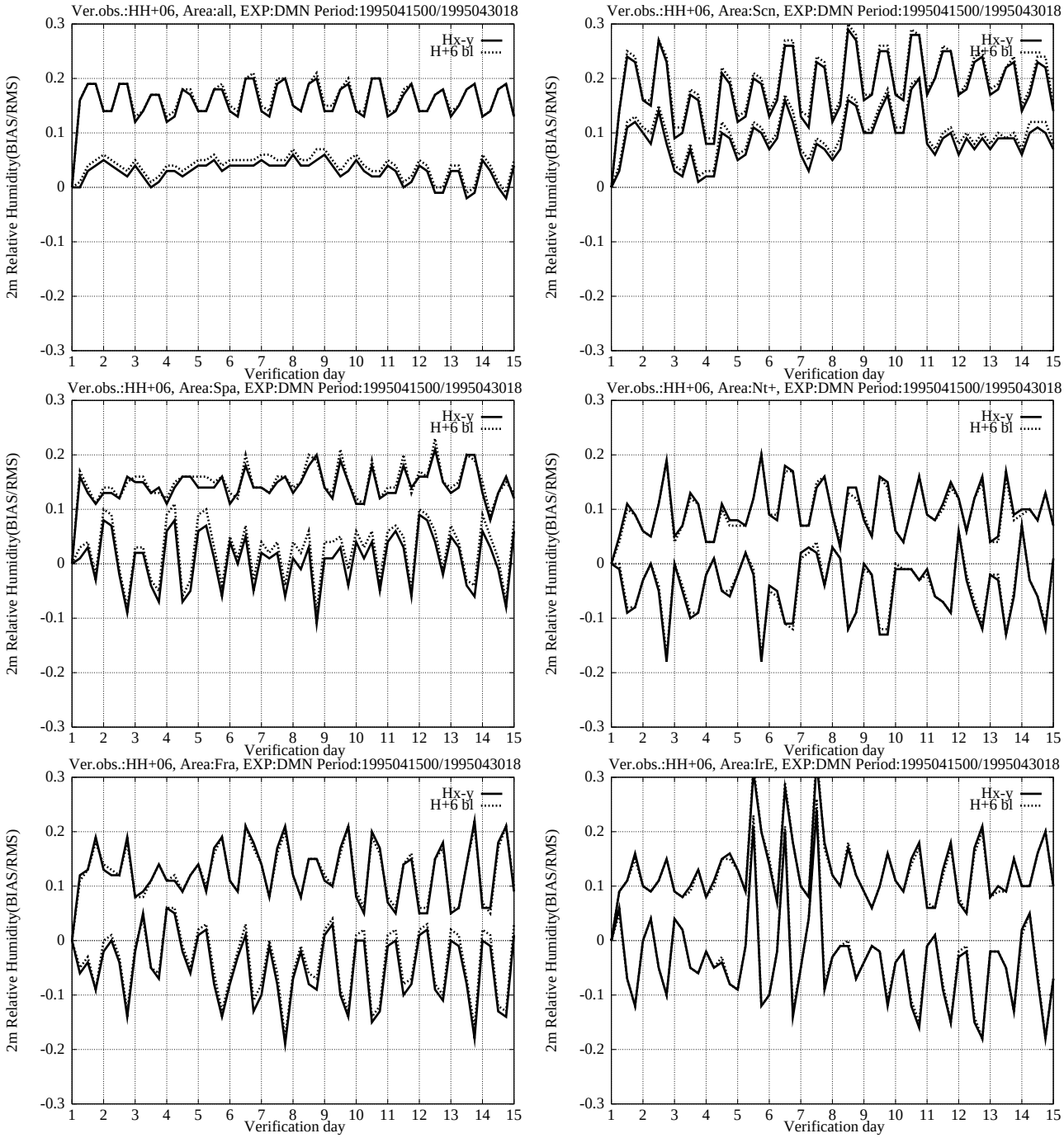

Figure 3: As in Fig. 2, but for 2-metre relative humidity.

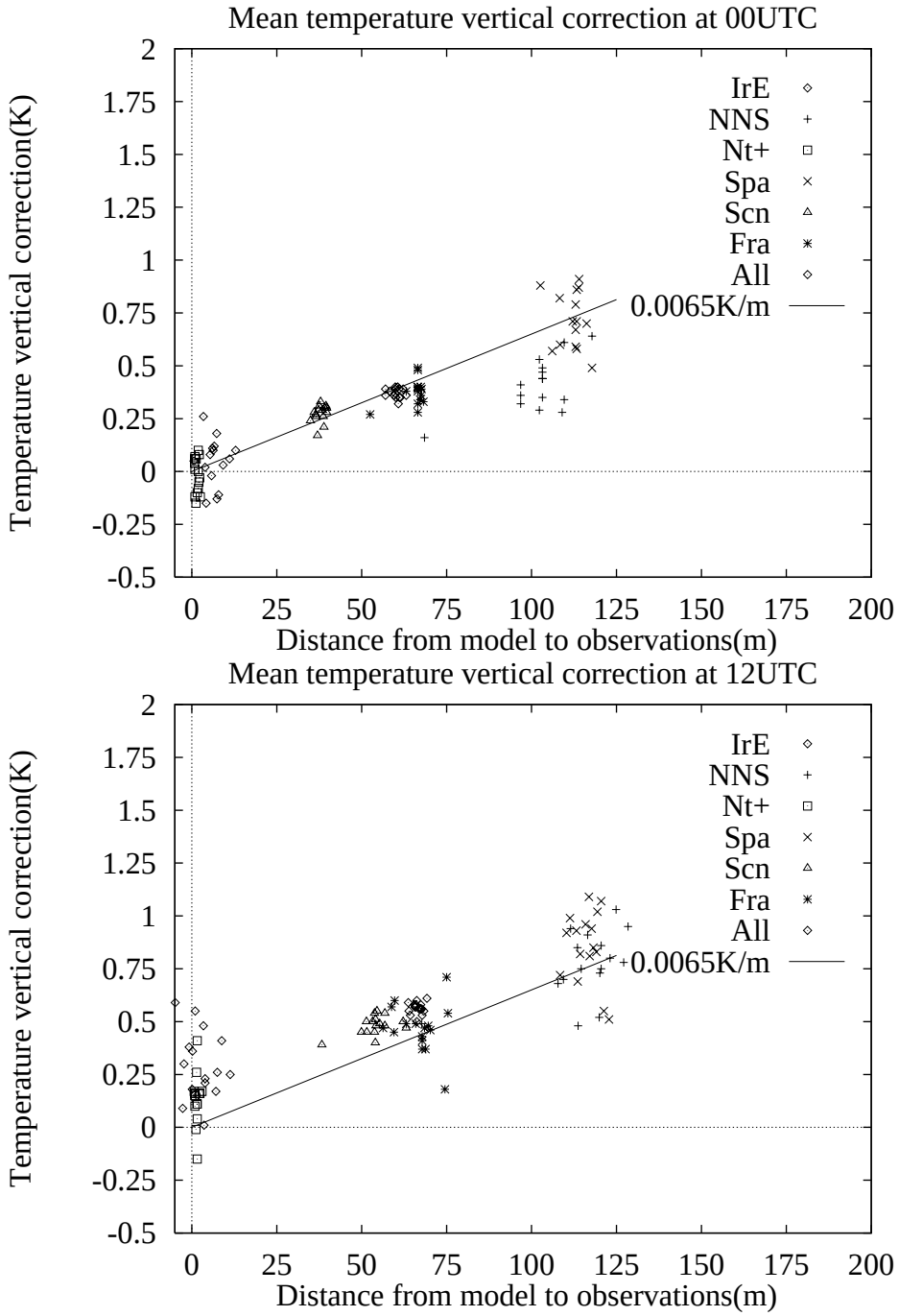

Figure 4: Average distance between station height and the corresponding model height versus difference in 2-metre temperature bias for the two verification strategies described in the text. Both differences in height and 2-metre temperatures are averaged for all stations within the reference system verification areas. Each figure corresponds to different verification time: 00 and 12 UTC. Each point within each figure corresponds to different verification dates over the period 15-30 April 1995.

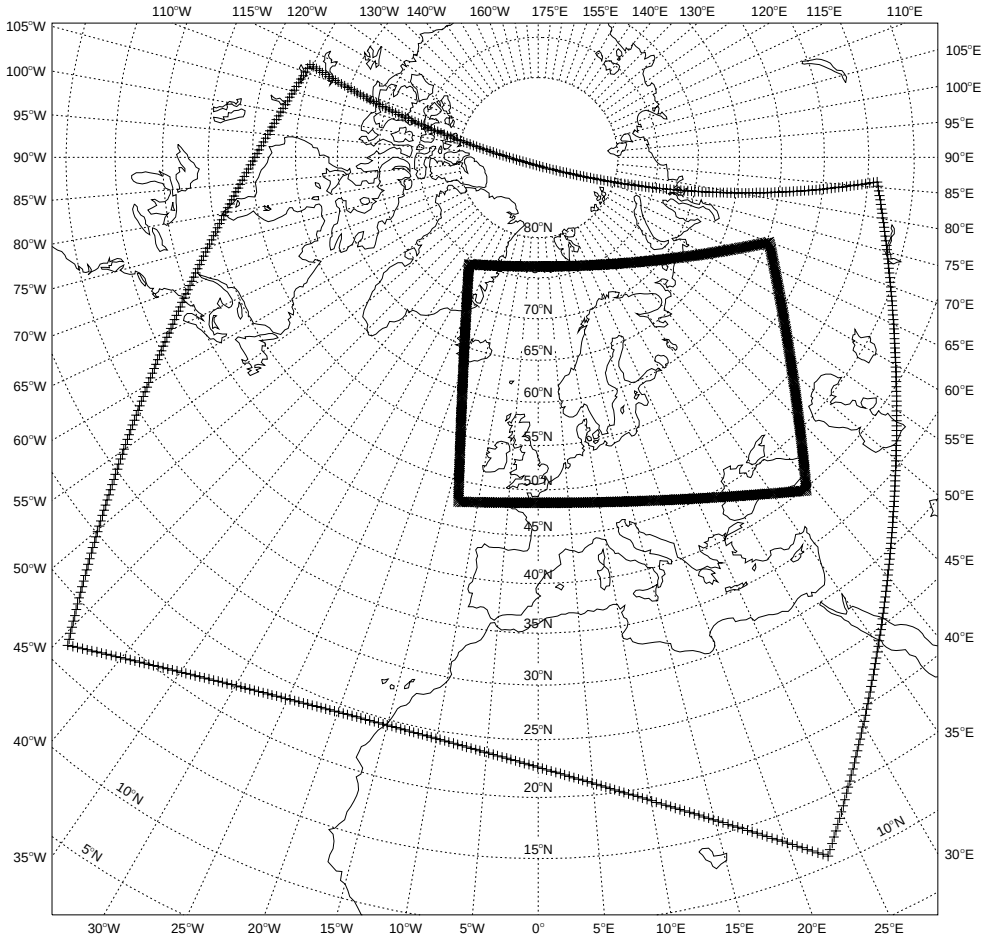

Figure 5: Domains used for parallel testing: i) DMR covering most of Europe and North Atlantic (0.5^o horizontal resolution); ii) FMI covering mainly a Nordic European area (0.2^o horizontal resolution).

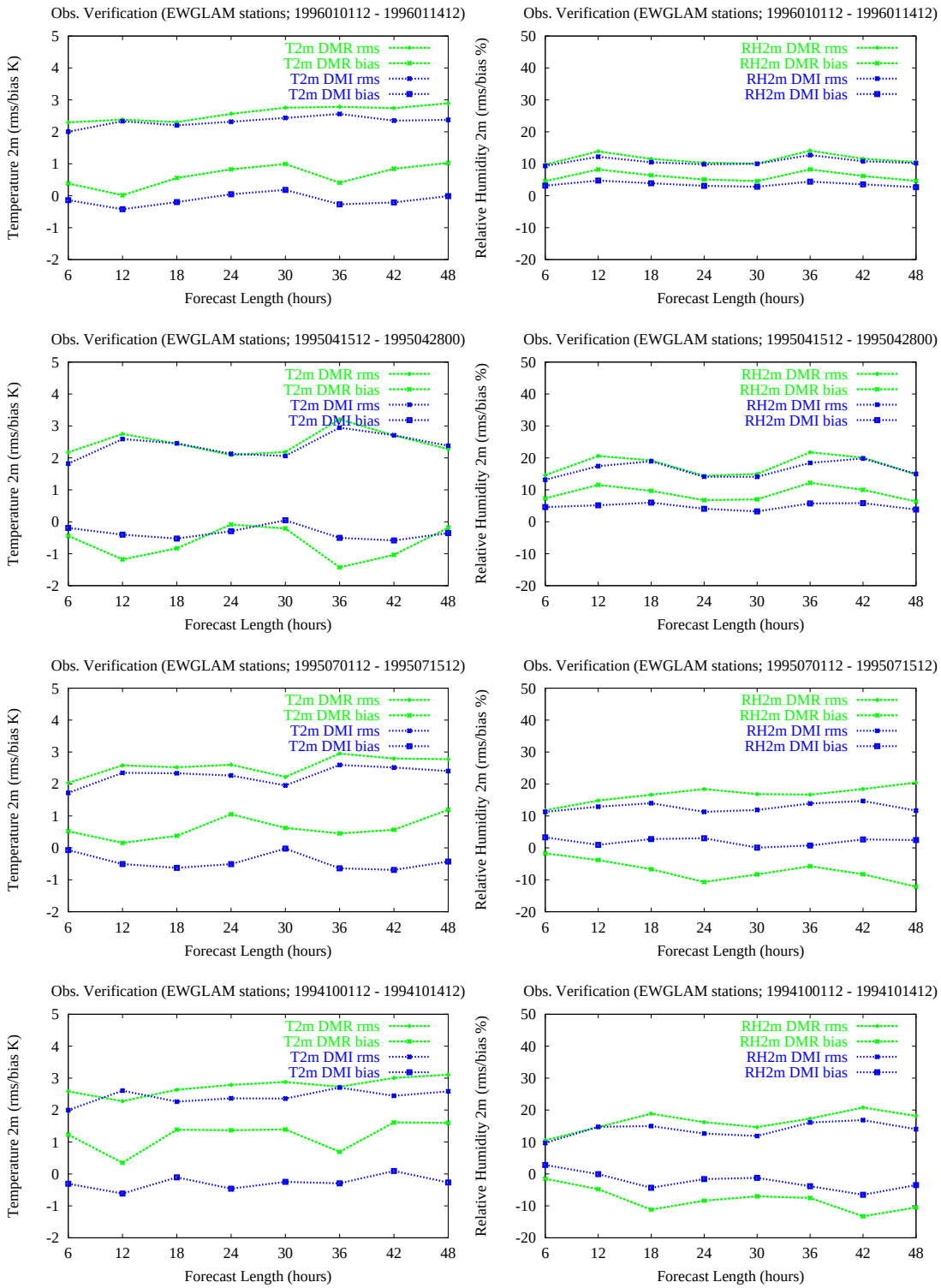

Figure 6: Bias and rms error as a function of integration range averaged for EWGLAM stations. All integrations start at 00 UTC: T_{2m} (left), RH_{2m} (right). Experiment DMR refers to version 5.1.1 and DMI to the new surface package on top of version 5.1.1. Each row corresponds to a different test period: 1^{st} row: 1-15 January 1996; 2^{nd} row: 15-30 April 1995; 3^{rd} row: 1-15 July 1995; 4^{th} row: 1-15 October 1994.

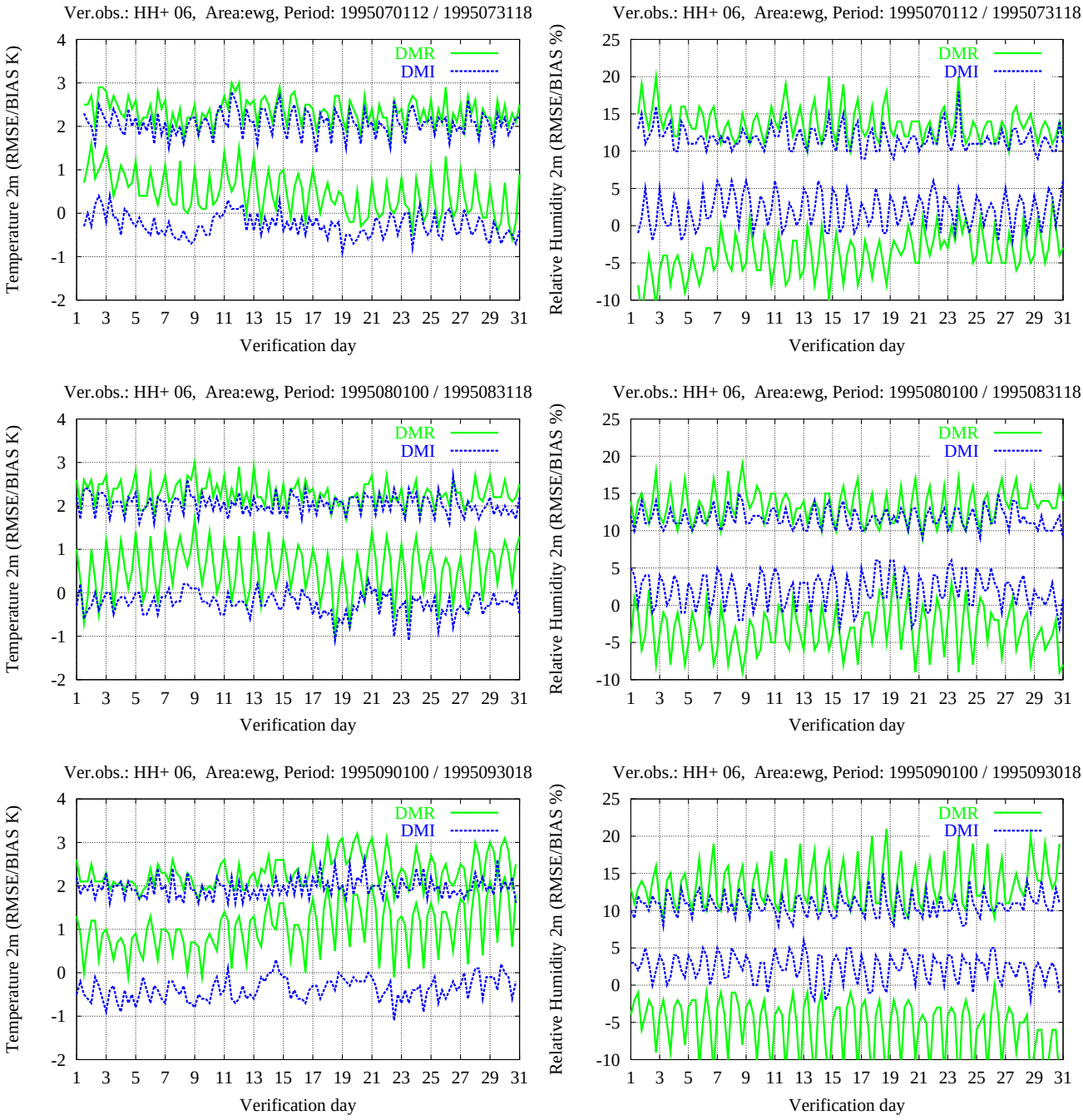

Figure 7: 2-metre temperature (left) and 2-metre relative humidity (right) bias/rms error of H+06 forecastings. Experiment DMR refers to version 5.1.1 and DMI to the new surface package on top of version 5.1.1. July 1995 (top), August 1995 (middle), September 1995 (bottom).

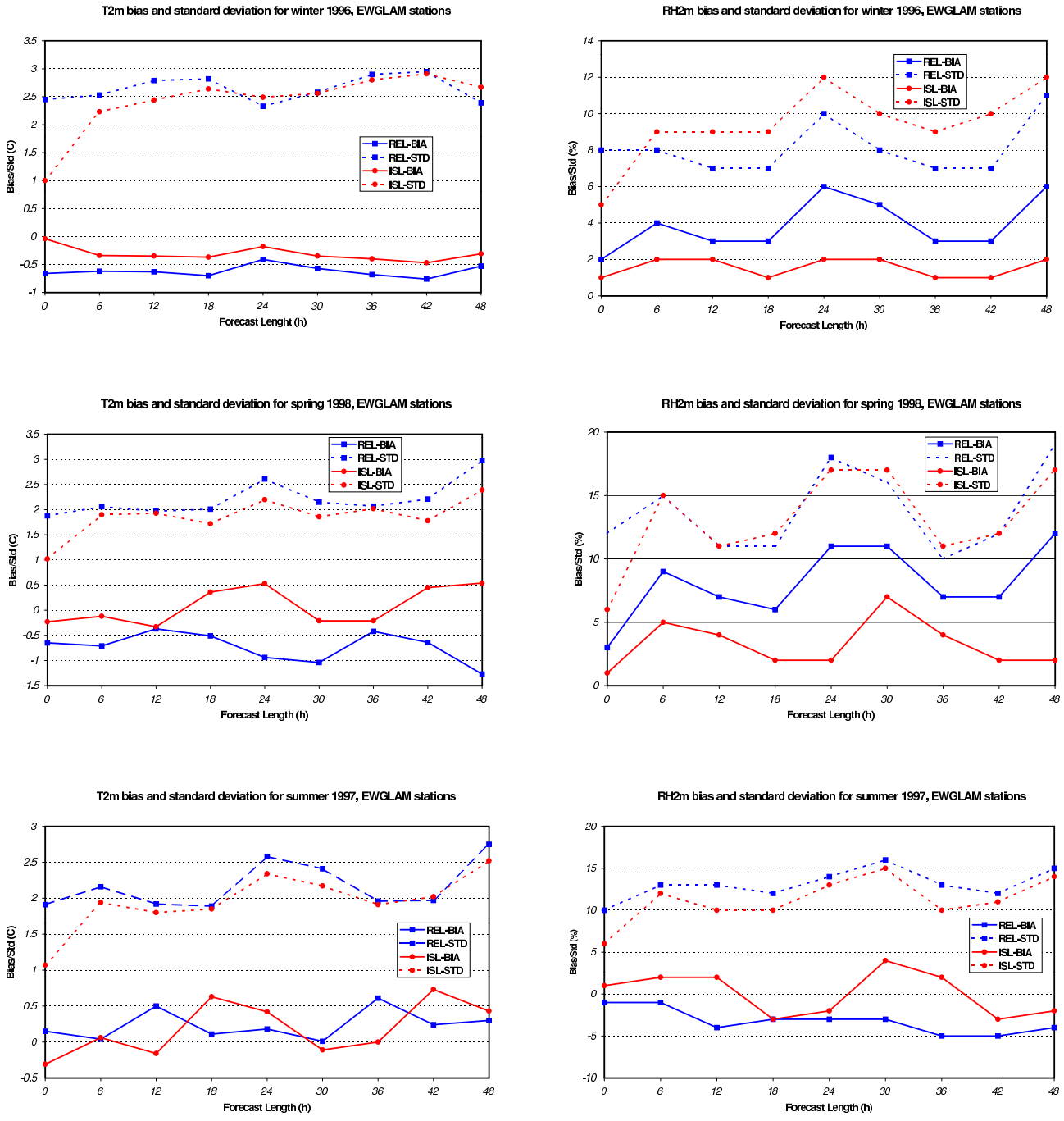

Figure 8: T_{2m} (left) and RH_{2m} (right) bias (full lines) and standard deviation (dashed lines) as a function of forecast length for REL (square) and ISL (circle) experiments. All integrations start at 12 UTC. Each row corresponds to a different test period: 1^{st} row: 1-15 January 1996; 2^{nd} row: 12-26 April 1998; 3^{rd} row: 6-17 June 1997.

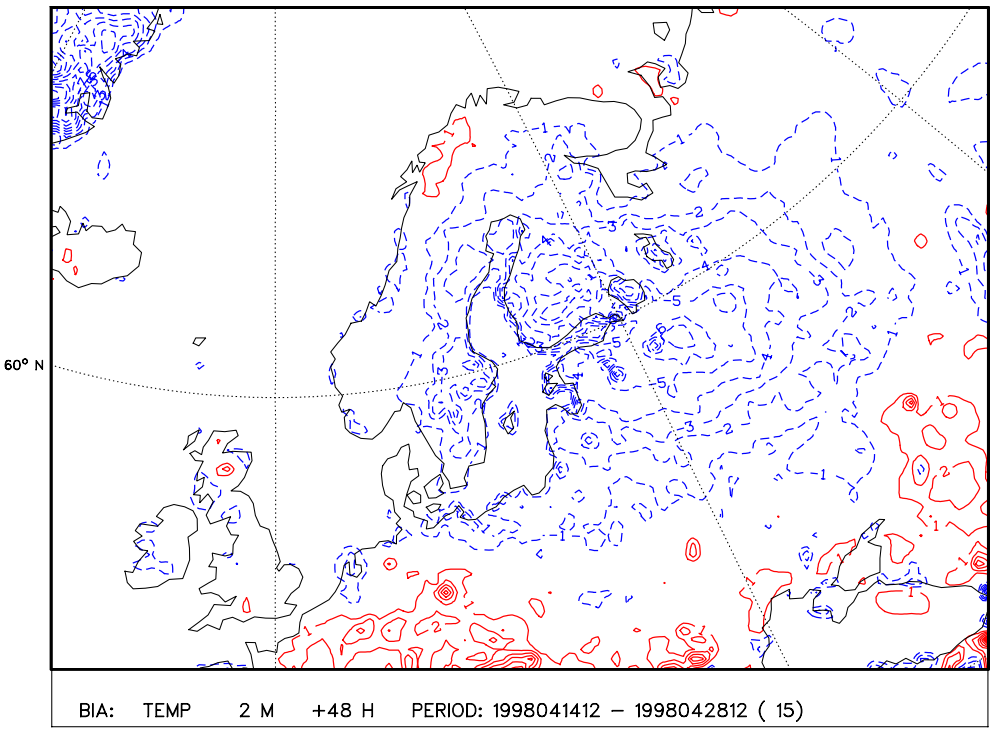

Figure 9: T_{2m} forecast error (forecast-analysis) in the 48 h forecasts (valid at daytime) for REL experiment, 12-26 April 1998. Contour interval: 1°C. The zero isoline not plotted, negative values indicated with dashed lines.

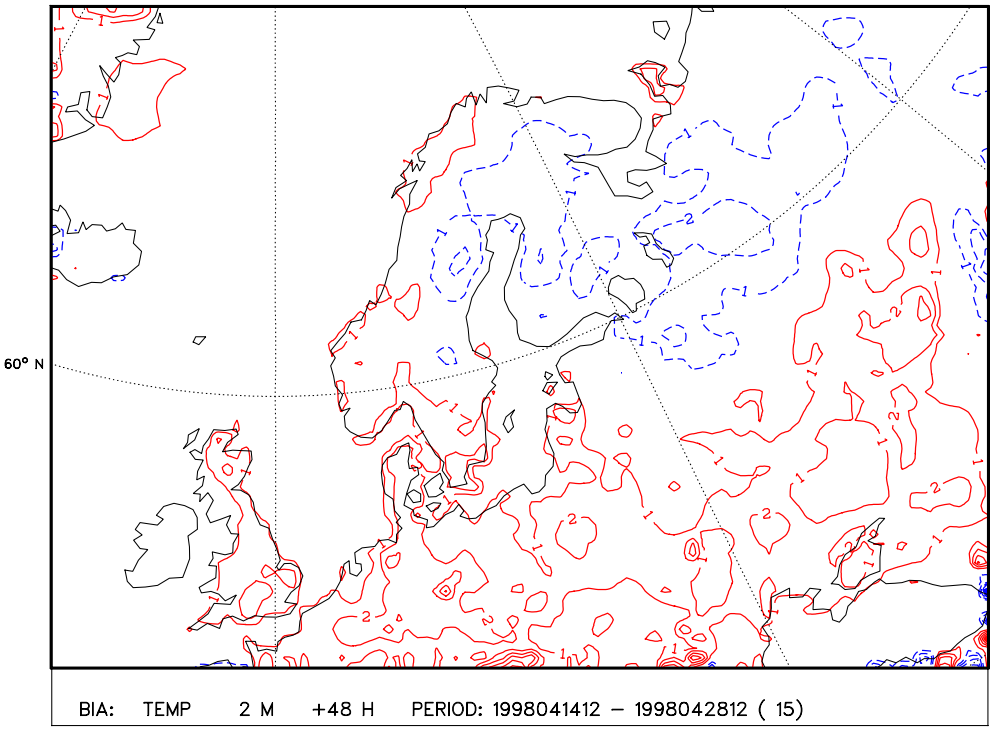

Figure 10: T_{2m} forecast error (forecast-analysis) in the 48 h forecasts (valid at daytime) for ISL experiment, 12-26 April 1998. Contour interval: 1°C. The zero isoline not plotted, negative values indicated with dashed lines.

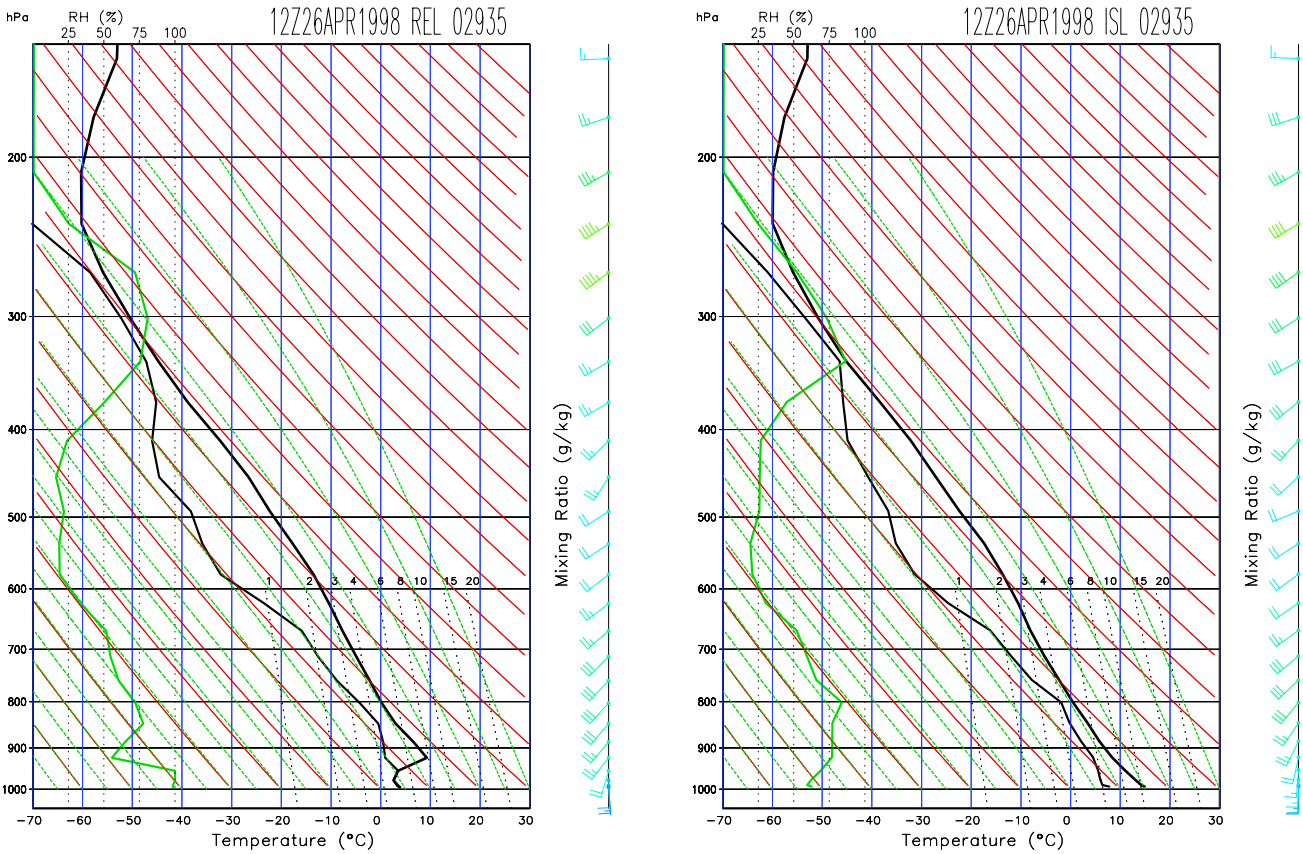

Figure 11: Forecast (+24 h) model profiles valid at 12 UTC 26 April 1998 for a grid point close to the Luonetjärvi station in central Finland, REL (left) and ISL (right).

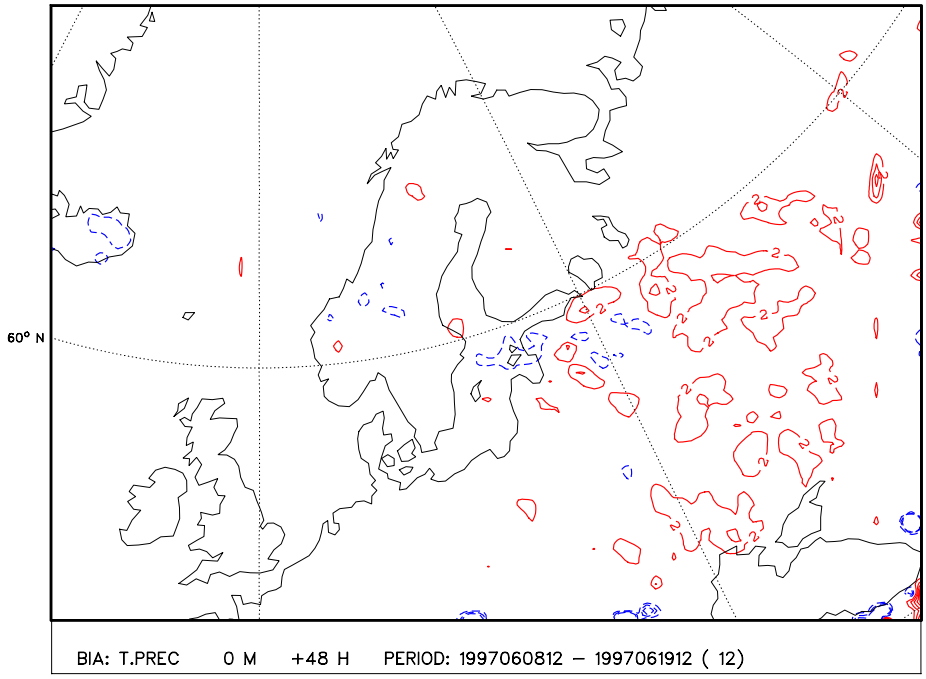

Figure 12: Systematic difference in 48 h accumulated precipitation between ISL and REL (ISL-REL) experiments, 6-17 June 1997. Contour interval: 2 mm. The zero isoline not plotted, negative values indicated with dashed lines.

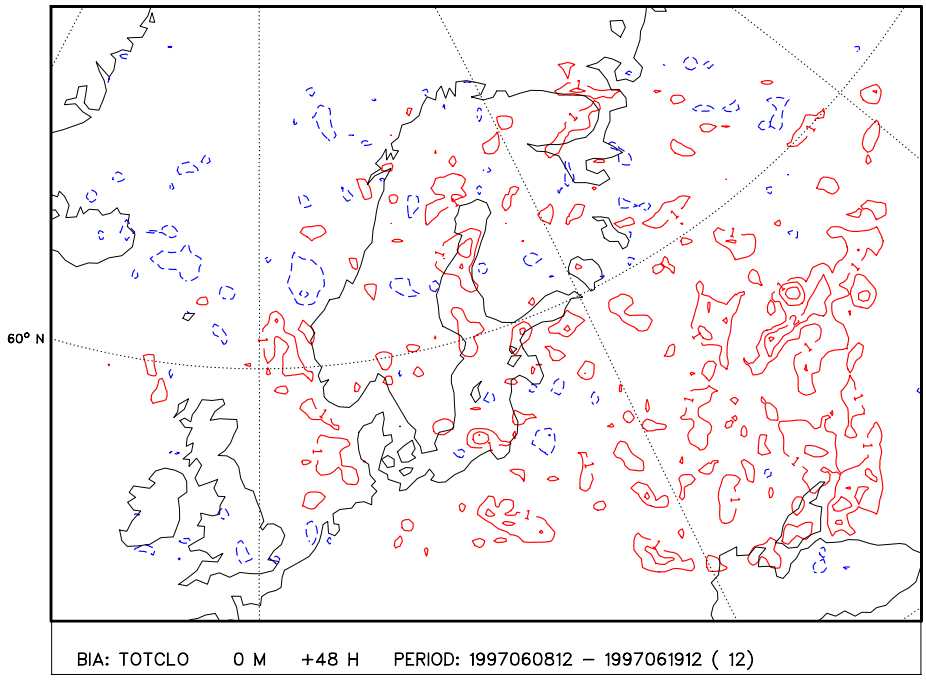

Figure 13: Systematic difference in 48 h (daytime) total cloud cover between ISL and REL (ISL-REL) experiments, 6-17 June 1997. Contour interval: 1 octa. The zero isoline not plotted, negative values indicated with dashed lines.